The Role of North Atlantic Deep Water Formation in an OGCM's Ventilation and Thermohaline Circulation*

PAUL J. GOODMAN

Department of Atmospheric Sciences, University of Washington, Seattle, Washington

(Manuscript received 14 April 1997, in final form 9 December 1997)

ABSTRACT

Two coarse-resolution model experiments are carried out on an OGCM to examine the effects of North Atlantic Deep Water (NADW) formation on the thermohaline circulation (THC) and ventilation timescales of the abyssal ocean. An idealized age tracer is included to gauge the ventilation in the model. One experiment is forced with the present-day climatology, the other has a negative salinity anomaly imposed on the North Atlantic surface to eliminate the formation of NADW. The Atlantic branch of the THC is reversed and the ventilation of the deep Atlantic basin is severely reduced when NADW formation is prevented. The Southern Ocean forms bottom water in both experiments, but downwelling and upwelling in the Southern Ocean are both reduced when NADW is included due to increased stratification of the water column. The Indian and Pacific basins are upwelling regions in both experiments and upper-level upwelling is stronger there when NADW is included; this change leads to cooler temperatures and reduced ventilation of the upper ocean.

There is a need for the distinction to be drawn between upwelling, the vertical movement of water parcels, and positive buoyancy forcing, which converts denser water masses into lighter ones. A density-regime analysis reveals that most of the positive buoyancy forcing associated with the THC occurs equatorward of 30° latitude in both hemispheres. The THC in the model ocean seems more modular than the ''conveyor belt'' metaphor implies; each high-latitude region functions quasi-independently, responding to its own heat and freshwater forcing. The newly ventilated subsurface water masses formed in each region compete for space in the water column. The production of NADW increases the upper-level stratification throughout the World Ocean. The idealized age tracer reveals that the deep Pacific and Indian basins are primarily ventilated by southern bottom water and the inclusion of NADW causes only minor changes. The qualitative pattern of ventilation in the model is determined by the number and location of subsurface water mass formation regions; the actual ages in the deep ocean are very sensitive to the vertical diffusion prescribed in the model.

1. Introduction

The processes and timescales associated with the ventilation of the deep and middepth ocean continue to be major unresolved questions in both oceanography and climatology. Much work has been done to date, both through observational analysis and computer modeling, but as yet no consistent, geographically complete description exists. While it is known that new bottom and deep waters are created in the high-latitude Southern Ocean and North Atlantic as part of the global thermohaline circulation, the ventilation of the abyssal and middepth ocean away from these formation regions is still poorly understood. With the possible threat of global climate change due to anthropogenic factors, understanding of the ocean's potential to ameliorate or enhance these stresses is of critical concern.

The current description of the ocean's thermohaline circulation (THC), the so-called global conveyor belt as put forth by Broecker (1987, 1991, 1995), Gordon (1986, 1991), and others, suggests that it is driven primarily by convection in the North Atlantic. North Atlantic Deep Water (NADW) advects a great quantity of salt into the Southern Ocean and the Antarctic Circumpolar Current (ACC). The salinity-enhanced Circumpolar Deep Water (CDW) briefly upwells, loses its heat to the atmosphere, and sinks to the bottom as Antarctic Bottom Water (AABW). Elsewhere, deep and bottom waters absorb heat diffusively, upwell gradually, and eventually return to the sinking regions.

A study by Schmitz (1995, S95 hereafter) reviewed much of the observational evidence from a wide variety of sources and compiled a coherent summary of the global THC. This report concluded that NADW is first converted into CDW, and it is this water mass that then fills the deep Indian and Pacific basins. It is notable in the S95 analysis that the only region in which upper water is converted into deep water is the North Atlantic

* Joint Institute for the Study of Atmosphere and Ocean Contribution Number 436.

Corresponding author address: Paul J. Goodman, JISAO, University of Washington, Box 354235, Seattle, WA 98195-4235.
E-mail: pgoodman@atmos.washington.edu

and that all bottom water is converted from CDW. Contrary to S95, however, recent work by Peacock and Broecker (1998) concluded that the only way to explain the phosphate star (PO_4*) evidence (see Broecker et al. 1991 for discussion) is if equal volumes of Antarctic surface water and North Atlantic surface water are converted into deep or bottom water. Observational studies (Carmack and Foster 1975; Foster and Carmack 1976; Foster 1995) have located only about one-third as much bottom water formation at various sites along the coast of Antarctica compared to the estimated rate of NADW formation, but large uncertainties due to the analysis technique, as well as potential spacial and temporal variability, still exist. S95 also concluded that all deep water upwelling occurs in the Indian Ocean and the Southern Ocean, although he acknowledged that the vertical exchange processes in the Indian and Pacific Oceans are poorly established.

Sedimentary evidence ($\delta^{13}C$) indicates that NADW production was less plentiful, if not entirely eliminated (Boyle and Keigwin 1987) during the last glacial period than at present, while AABW production (or rather, strong convection between the surface and deep water in the Southern Ocean) was comparable or more vigorous (Duplessy et al. 1988). Modeling results consistently indicate that AABW production remains roughly constant whether or not NADW production is present (Fichefet et al. 1994; Stocker et al. 1992; England 1993; Cai and Greatbatch 1995). Radiocarbon evidence ($\Delta^{14}C$) also indicates that water in the deep, tropical Pacific was about 70 ± 105 years older relative to the surface during the last glacial period than at present (Broecker et al. 1990; Duplessy et al. 1992).

This highlights an obvious question: if NADW production and export is the main process behind the ventilation of the abyssal ocean, then how could the deep Pacific Ocean experience such a small change in deep water ages at a time when NADW production was sharply curtailed? The obvious alternative is that the formation of recently ventilated AABW occurred independently of NADW production during the last glacial period, and the deep Pacific was ventilated by AABW. The role of AABW in the global THC and ventilation of the deep ocean has been largely ignored or deemed secondary in importance to that of NADW.

The present study will examine this question in an OGCM simulation under two related, yet distinct, sets of boundary conditions: one which includes NADW production and one in which this critical water mass is eliminated. The purpose of this study is twofold: to provide a thorough analysis of the model's circulation, in terms of mass transport and density regime conversion, and to distinguish between these two processes; and to present a coherent description of the model's THC in order to examine the role of NADW on the global overturning. It should be noted that water masses in OGCMs are generally not equivalent to the real-world water masses in terms of their temperature and salinity characteristics. The model water masses discussed in this paper are given the same names as their real counterparts because they seem to function the same in the context of the model circulation.

An idealized passive age tracer is included to gauge the ventilation timescales throughout the model ocean. The idealized age tracer used in these experiments is derived from that of Haidvogel and Bryan (1992) and was recently incorporated into an OGCM by England (1995); it gives an indication of the time elapsed since a fluid parcel was last at the surface. Since the ''atmosphere'' plays no role in its final structure, the age profile derived from this idealized age tracer is solely dependent on the model circulation. In this regard, it can serve as a benchmark against which to compare the oceanic portion of various modeling efforts.

Modeling studies of the ocean's general circulation provide a wealth of information not currently obtainable from the real ocean. Due to the lack of hard numbers needed to evaluate or contradict model performance, however, most researchers have concentrated on process studies or sensitivity studies, or have limited their analyses to those particular features where observational data have been recorded. Rigorous analyses of model results are useful in and of themselves, in that all relevant data is available; until we can understand model results more completely, we cannot hope to describe fully the more complex, real-world ocean. The intercomparison of different models, model configurations, and parameters, and boundary conditions provides essential information about the models and may be the only way to increase our confidence in the simulations they provide. They also can guide observational studies to opportune geographical locations for data collection. Accordingly, many of the physical features simulated by the model will be discussed quantitatively, despite the paucity of data regarding the deep ocean circulation.

Results indicate that the largest effects of NADW formation are found in the Atlantic, but there are distinct and important changes to the rest of the World Ocean as well. Contrary to the standard picture of a single ''global conveyor,'' the model ocean basins seem to function quasi-independently, with each northern basin and the Southern Ocean responding to its own high-latitude heat and freshwater balance. Water of southern origin fills the deepest model levels regardless of the presence or absence of NADW. Most of the upwelling in the model occurs in the circumpolar region, but most of the positive buoyancy forcing occurs between 30°S and 30°N. Low-salinity southern subpolar intermediate water is much more prevalent throughout the World Ocean when NADW is removed. NADW formation also affects the upper-level upwelling in the Indian and Pacific; intermediate waters there are both colder and less ventilated (older) when NADW production is included.

The structure of the paper is as follows: section 2 describes the model formulation; section 3 presents the global circulation for the Control experiment; section 4

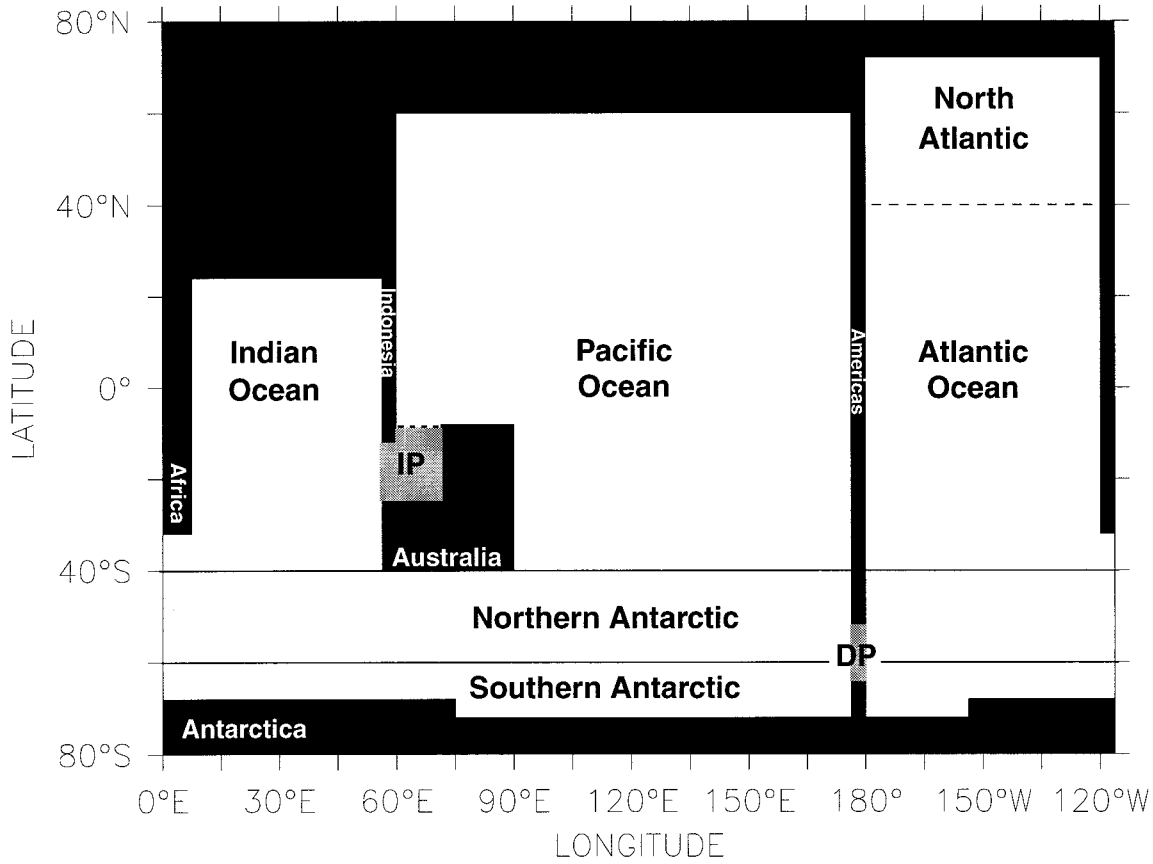

FIG. 1. The model domain. Names indicate regions referred to in this study and are adopted from Cox (1989). DP refers to the location of Drake Passage; IP: the Indonesian passage. Southern Ocean in the text refers to both the northern and southern Antarctic, while the ''high latitude'' Southern Ocean refers to the southern Antarctic only.

presents the global circulation in the model when NADW formation is artificially eliminated (referred to as the No-NADW experiment); a cartoon depicting the model's THC is presented in section 5 that summarizes the results and offers some conclusions.

2. The model

a. Geometry

The experiments are carried out on the GFDL Modular Ocean Model (Pacanowski et al. 1991) in an idealized topography. The geometry (Fig. 1) consists of three basins to represent the Indian, Pacific, and Atlantic Oceans, along with a reentrant channel in the south that allows for the formation of an ACC. The total zonal extent of the model is 240°; the Indian and Atlantic basins span 60° of longitude, and the Pacific covers 120°. The southern extreme of the model is 72°S, and the northern extremes for the Indian, Pacific, and Atlantic Oceans are 24°N, 60°N, and 72°N, respectively. The grid spacing is coarse: 3.75° (zonal) by 4° (meridional). The geometry includes a representation of Australia and an Indonesian passage. Both Australia and Antarctica are treated as true islands and the model calculates the barotropic transport around them.

The bathymetry is divided into 20 levels of increasing thickness from 50 m at the surface to 449 m at the bottom, making up a total of 5000 m everywhere. There is no bottom topography except in Drake Passage where the sill depth is 2500 m and in the Indonesian passage where there is a plateau at 1551 m. This idealized geometry captures the basic elements necessary to differentiate among the distinct ocean basins and to simulate a global thermohaline circulation within the constraints of the model resolution.

b. Surface forcing

Restoring boundary conditions for both temperature and salinity are applied at the surface with a Haney-type restoring scheme (Haney 1971) using a fixed restoring timescale of 50 days. Zonally and annually averaged quantities from the 30-m level of the Levitus (1982) climatological atlas are used, with some modifications. The global zonal average is applied south of 40°S; the Levitus data is fairly uniform along the latitude

circles there. North of 40°S, each basin is forced with its own zonal average. North of 60°N in the Atlantic, the restoring salinity is calculated from the values east of Greenland only. Labrador Sea surface salinities are much lower and their inclusion in the basin average severely restricts the formation of northern deep water in the model. The other modification to the Levitus dataset is to smoothly increase the restoring salinity off the Antarctic coast from climatology at 60°S to 35 psu at 70°S, as was done by England (1993). Together, these changes create a reasonable balance between deep-water production in both hemispheres and simulate the global salinity profile more accurately than the enhancement of either hemisphere alone or no enhancement at all. It must be noted that observational studies near Antarctica have indicated the importance of shelf processes in the formation of AABW (Foster 1995); these processes are not explicitly modeled in this or most other OGCM simulations.

Toggweiler and Samuels (1995) stated that the use of artificially high restoring salinities over the high-latitude Southern Ocean induces a surface freshwater flux that implies a rate of ice formation and export much higher than observed. They attribute the poor salinity structure in coarse-resolution models to a failure of the modeled NADW to transport enough salt into the ACC. Duffy and Caldeira (1997), however, report that the simulation of the global salinity profile is greatly enhanced, without affecting the diagnosed freshwater flux, when the salt rejected from Antarctic sea ice formation is incorporated into the top 160 m of the water column instead of the surface box alone. It is known that the Antarctic data in the Levitus dataset was collected in the austral summer and as a result, the upper-level salinities are excessively fresh compared to the deep water in this location (Levitus 1982). The restoring salinities used in this experiment are closer to the observed deep-water characteristics. Since the focus of this paper is not on the diagnosed salinity flux, this modification is considered appropriate.

To test the sensitivity of the model to the enhanced salinities in both the North Atlantic (GIN seas salinity only) and the high-latitude Southern Ocean, various runs were conducted with either one enhancement or the other or neither. When neither hemisphere was enhanced, that is, when using the actual Levitus data, the global circulation was similar to the one discussed in this paper, but the globally averaged vertical salinity profile was exceedingly fresh. When the enhancement was applied to only the Northern Hemisphere, the Southern Hemisphere still produced deep water, but the global deep and bottom salinities were still too fresh (about 0.5‰ lower than observed), and the rate of NADW formation was much larger than observed [over 28 Sv (Sv $\equiv 10^6$ m^3 s^{-1})]. Increasing the Antarctic surface salinities, while including the Labrador Sea salinities in the North Atlantic restoring salinity value, caused North Atlantic Deep Water production to cease. Further sensitivity studies focused on the bathymetry and boundary conditions, as well as the effect of sea ice in the Antarctic sector are needed.

TABLE 1. Ocean model parameters.

Parameter	Value
Horizontal diffusivity	1×10^7 cm^2 s^{-1}
Horizontal viscosity	6×10^9 cm^2 s^{-1}
Vertical diffusivity	0.3–1.1 cm^2 s^{-1}
Vertical viscosity	1.0 cm^2 s^{-1}
Surface relaxation time ($1/\tau$)	
Temperature and salinity	50 days
Passive age tracer	0 days

The zonal component of the zonally and annually averaged wind stress from Hellerman and Rosenstein (1983) is applied uniformly at all longitudes. No meridional wind stress is applied anywhere. The model employs no-slip boundary conditions at the walls and there is no bottom friction. Viscous and diffusive mixing are prescribed in a Cartesian frame with constant coefficients, except for the vertical diffusivity, which varies from 0.3 cm^2 s^{-1} at the surface to 1.1 cm^2 s^{-1} at the bottom. It is parameterized by a depth-dependent function identical to that of Robitaille and Weaver (1995), which is based on, but different from, the original formula presented in Bryan and Lewis (1979). All the parameters employed in these experiments are given in Table 1.

c. Idealized age tracer

The idealized age tracer used in these experiments was suggested by Haidvogel and Bryan (1992). The surface age is set to zero everywhere at each time step, equivalent to a zero-day restoring timescale. At each internal grid box, the age tracer act likes a running clock with time being added at each time step, according to the formula:

$$\mathrm{AGE}(t + \Delta t) = \mathrm{AGE}(t) + L(t) + \Delta t, \qquad (1)$$

where t is time, Δt is the length of the model time step, and L represents all the advection and mixing from adjoining grid boxes. The idealized age tracer acts like a stopwatch that is reset at the surface and keeps track of the time after a parcel descends into the water column, rather than modeling a decaying quantity, such as ^{14}C, which must be compared to a reference value to determine the elapsed time. By removing the need for an arbitrary reference, it is closer to a Lagrangian estimate of the average time elapsed since a parcel was at the surface and does provide an accurate indication of ventilation times in the model.

Sensitivity studies indicate that the qualitative pattern of ages is primarily a function of the surface forcing, that is, the number and location of deep-water sources. Away from the convecting regions, however, the mod-

eled ages are highly sensitive to the parameterization of the vertical diffusion employed. It should be noted at this point that ''ventilation'' is defined as the process of moving a parcel of water from the surface to a given subsurface location and ''ventilation age'' or ''age'' as the time it takes to get to a given location from the surface. Ventilation can occur through convection, subduction, advection, and diffusion.

d. Experiments

In the Control experiment, NADW formation is observed when the model is forced at the surface with present day climatological values. In the No-NADW experiment, NADW formation is halted by imposing a negative salinity anomaly on the North Atlantic north of 40°N, which nearly eliminates the convective activity in this region. The low salinity anomaly is imposed by reducing the previously mentioned restoring salinity values over this sector by 1‰ and letting the model achieve a new steady state. Many studies have explored the existence of multiple equilibria in OGCMs (e.g. Manabe and Stouffer 1988; Marotzke and Willebrand 1991; Power and Kleeman 1993; Hughes and Weaver 1994; and others), but the present study does not fall into this category. Multiple equilibria, by definition, exist under identical forcing: the steady-state equilibrium being determined solely by the initial conditions. As stated above, the purpose of this study is to compare and contrast the two *differently forced* steady states, without delving into how the system gets from one equilibrium to the other. This transition will be the subject of future work.

3. Control experiment (with NADW)

Under the control (i.e., present day) forcing, the model produces many of the features observed in today's ocean. Deep water is formed in both hemispheres (Fig. 2a), driven by high-latitude convection (Fig. 2b). A strong ACC develops with a transport of 205 Sv through Drake Passage (Fig. 2c). This value is higher than the observed estimates of 125 Sv (±15 Sv) (Whitworth et al. 1982) but is typical of OGCM results (Semtner and Chervin 1988; Hirst and Godfrey 1993; Cai and Greatbatch 1995). The flow through the Indonesian passage from the Pacific into the Indian basin measures 22.2 Sv (Fig. 2c), again higher than the observations [extrema in the throughflow were reported by Fieux et al. (1996) as −2.6 Sv and 18.6 Sv westward flow, and Meyers (1996) determined that ENSO-induced variability was ±5 Sv around a mean of 11 Sv], but in accord with other modeling results (Hirst and Godfrey 1993; England 1993; Cai and Greatbatch 1995) given the idealized model topography. The westward portion of the flow south of Africa, known as the Agulhas Leakage, extends down to 1550 m and measures 16.3 Sv with over 15 Sv of the transport in the upper kilometer. Although it is believed that the majority of the transport is in the form of baroclinic eddies that are not resolved by this model, Gordon et al. (1992) stated that there is still a large uncertainty in the Agulhas Leakage transport (3–20 Sv westward), which may be the result of a wide temporal variation in the flow itself and not an artifact of the observational method.

The globally averaged temperature and salinity profiles are plotted as a function of depth along with the Levitus (1982) profiles in Figs. 2d and 2e. As with most coarse-resolution OGCMs, the thermocline is too diffuse compared to the observations; the maximum error is about 2°C too warm at 600 m. The salinity profile is simulated well; the salinity minimum associated with Antarctic Intermediate Water (AAIW) is clear, although the upper-level halocline is also a bit too diffuse. The model's globally averaged temperature and salinity are 4.1°C and 34.72 psu, compared to the Levitus (1982) averages of 3.4°C and 34.73 psu.

a. Antarctic sector

As seen in Fig. 2a, a net of 27 Sv sinks below 2500 m in the southernmost grid box, loosely corresponding to the Ross and Weddell Seas. This Antarctic overturning is slightly weaker than other modeling results [~34 Sv in Cai and Greatbatch (1995) and over 40 Sv in England (1993)] despite the enhanced restoring salinity. The sinking, south of 68°S, is divided into three regimes: the Weddell Sea in the Atlantic sector transports about 29 Sv downward; the southeastern Ross Sea between model longitudes 157°E and 180° in the Pacific sector transports about 29 Sv downward; and the southwestern and central Ross Sea is an upwelling region that carries 31 Sv of deep and bottom water toward the surface. A large percentage of the water downwelled west of the Antarctic Peninsula flows westward along the coast at the bottom and most of this upwells in the Indian and Pacific sectors of the high-latitude Southern Ocean. The meridional overturning (Fig. 2a), south of 60°S, conceals stronger, zonal overturnings in both the Indo–Pacific sector and the Atlantic sector of 55 and 27 Sv (measured at 2500 m), respectively.

The vertical transport is upward nearly everywhere between 68° and 60°S, except along the northwestern edge of the Antarctic Peninsula. As many authors have proposed, the largest part of the model ocean's upward vertical transport occurs in the Antarctic sector of the model, south of 60°S (Broecker 1991; Gordon 1991; Toggweiler and Samuels 1993; Shriver and Hurlburt 1997). Contrary to the standard description presented by these studies, however, this vertical motion is generally not associated with the conversion of denser water masses to lighter ones. This will be discussed further in section 3d.

Despite these strong overturnings, a net of only 7.9 Sv actually flow northward across 60°S in the bottommost 1300 m. The meridional flow across this section

is divisible into the same three regimes as the vertical motion: 15.5 Sv move southward at 60°S in the Indian and western and central Pacific sectors to supply the upwelling; 9.8 Sv of newly downwelled water flow northward in the far eastern Pacific, immediately west of the Drake Passage sill; and 13.6 Sv flow northward across 60°S in the Atlantic. Nearly all of the bottom water formed in the Atlantic sector flows northward below the ACC into the basin as a deep western boundary current (Fig. 3), although a portion is entrained into the eastward flowing ACC.

The modeled ages and velocity vectors for the bottom 1320 m of the ocean (Fig. 3) show the paths by which bottom water travels northward into the individual basins. The youngest water is adjacent to Antarctica and is less than 100 yr old. The outflow regions from the downwelling in the Weddell and Ross Seas are obvious. The dominant feature in each of the northern basins is a western boundary current, and the youngest water in each ocean is located near 30°S along the western boundary. Bottom water in the Atlantic basin is younger than the other regions due to both the strong flow of newly formed AABW directly from the Weddell Sea and the ''insulating effect'' of young NADW directly above it in the water column. This is consistent with the results of Mantyla and Reid (1983), who found that ''true'' AABW is only found in the Atlantic, whereas bottom water in the Indian and Pacific Oceans is actually the densest component of CDW and therefore generally less recently ventilated.

Surface convection in the Southern Ocean (Fig. 2b) occurs in two main regions: adjacent to the Antarctic coast, as discussed above, and in a swath extending from the southern tip of South America to the southern Australian coast to the southern African coast. Convection in the subpolar Southern Ocean has a maximum depth of 1000 m at the South American coast, the main formation region for ''AAIW'' in the model, and a lesser maximum at the southwest corner of Australia. Most of the area between 60° and 50°S is stably stratified; the surface forcing cannot overcome the wind-driven upwelling of upper CDW in this region. Figure 4 shows the ages and velocity vectors at 600 m. The age minima in the vicinity of South America and Australia correspond to the maxima in convection. In the South Atlantic, wind-driven upwelling between 60° and 40°S brings recently ventilated lower water to this level.

The age structures and flow patterns near South America and Australia are quite similar. These sites are in the path of the ACC where convergence along the coast leads to the downwelling of surface water into the water column. The age minima at the land masses spread toward the west-northwest, as does the outflow from the convecting regions. This figure is reminiscent of those presented in Hirst and Godfrey (1993, their Figs. 8b, 9b, and 10a); whenever the model ACC is influenced by a meridional wall, the flow develops a characteristic undercurrent structure (between 600 and 1000 m in depth), which they liken to the observed Leeuwin Undercurrent (in the southeastern Indian Ocean).

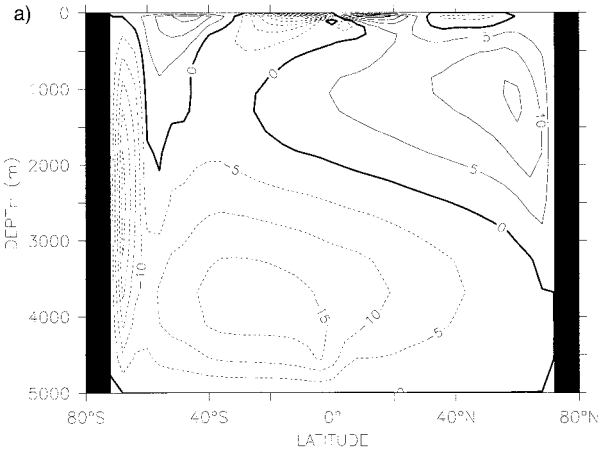

FIG. 2. Control experiment: (a) Meridional overturning streamfunction; contour interval is 5 Sv. (b) Depth of convection from the surface; contours at 50, 250, 500, 1000, 2500, and 5000 m, with the 500-m and 2500-m contours darkened. (c) Barotropic streamfunction; contour interval is 5 Sv, except in the ACC where it is 20 Sv. (d) Globally averaged temperature from the Control experiment (solid), No-NADW experiment (dashed), and Levitus (1982) (dotted); (e) Globally averaged salinity from the control experiment (solid), No-NADW experiment (dashed), and Levitus (1982) (dotted). Note that in (a) and (c) solid (dashed) contours denote clockwise (counterclockwise) circulation.

b. Atlantic sector

In the northeast Atlantic Ocean, 15.8 Sv are overturned down to 3000 m, again driven by convection (Fig. 2b), and 8.7 Sv of newly overturned water eventually cross 30°S, leaving the basin to join the ACC (Fig. 5). These values are similar to other modeling results (Manabe and Stouffer 1988; England 1993; Hirst and Godfrey 1993; Cai and Greatbatch 1995). More of the model's NADW upwells in the extratropical Atlantic than is reported in S95; his analysis indicates that all 14 Sv of the water downwelled in the North Atlantic flows southward out of the basin. This is a common shortcoming in OGCM experiments that employ Cartesian mixing: recent work by Böning et al. (1995) and Weaver and Eby (1997) has shown that the artificial upwelling due to the Veronis effect [anomalous upwelling on the coastal side of strong western boundary currents, Veronis (1975)] can be eliminated by the use of the Gent and McWilliams (1990) mixing parameterization. The effect of this parameterization on these results will be the subject of future work.

Below the North Atlantic cell, 7.2 Sv of southern bottom water (AABW) flow in across 30°S and 4.4 Sv eventually cross 30°N (see also Fig. 3). The first value is consistent with the hydrographic analysis by Speer and Zenk (1993) who found a 6.7-Sv northward flow of bottom water at 30°S, and the second with the ''best

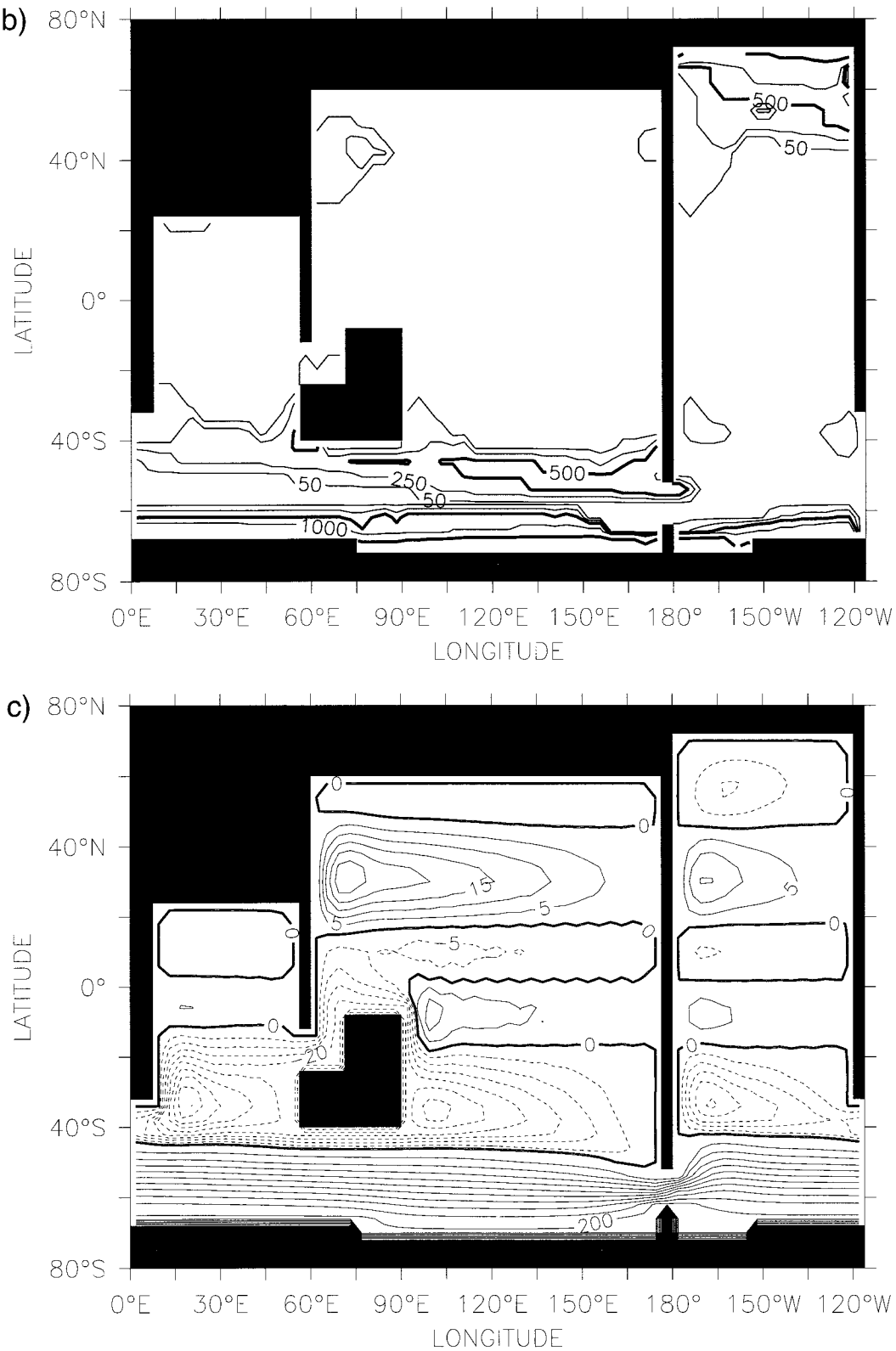

FIG. 2. (*Continued*)

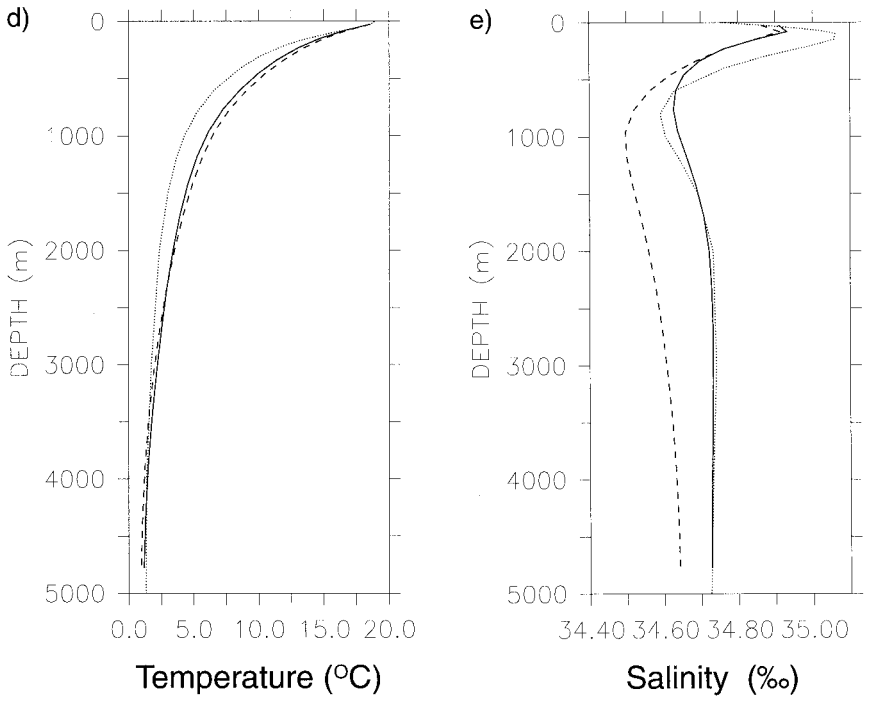

FIG. 2. (*Continued*)

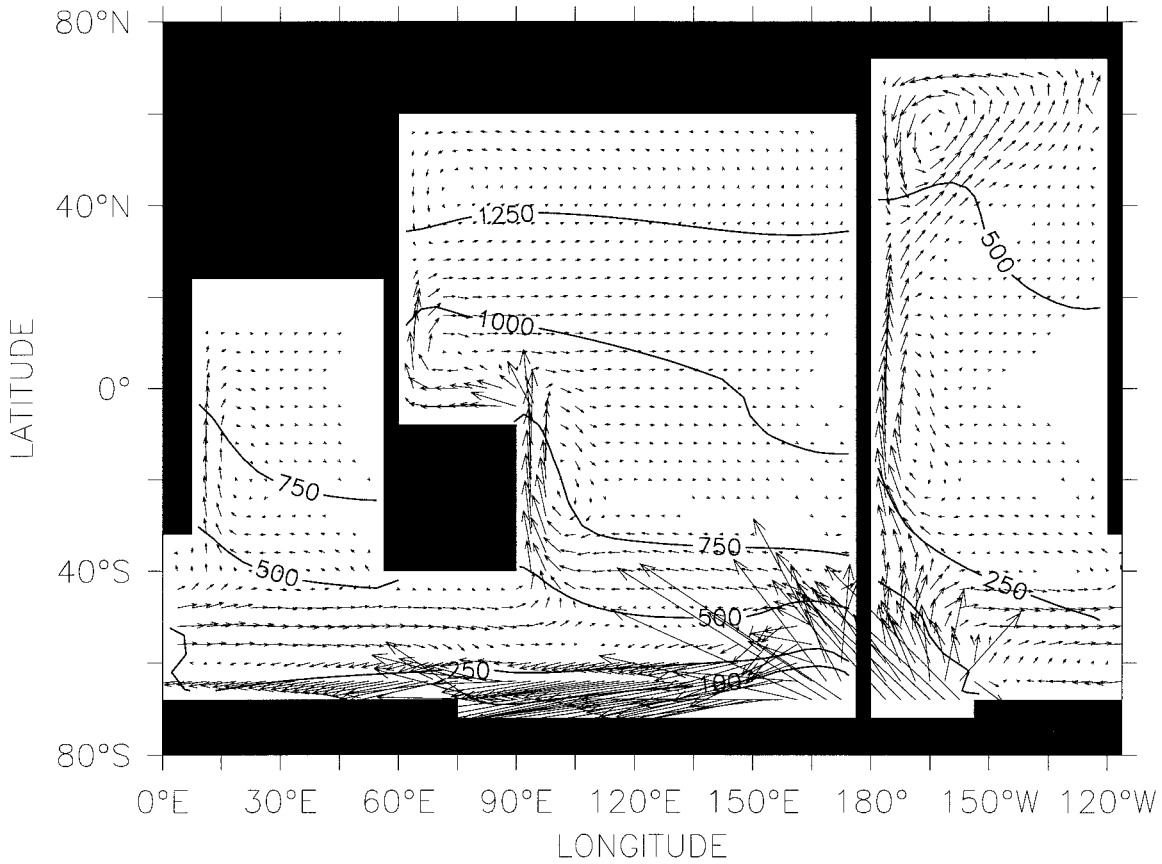

FIG. 3. Idealized ages and velocity vectors averaged over the bottom 1320 m of the water column (levels 18–20); contours are 100, 250, 500, 750, 1000, and 1250 yr. Maximum velocity vector in 4.10 cm s^{-1}.

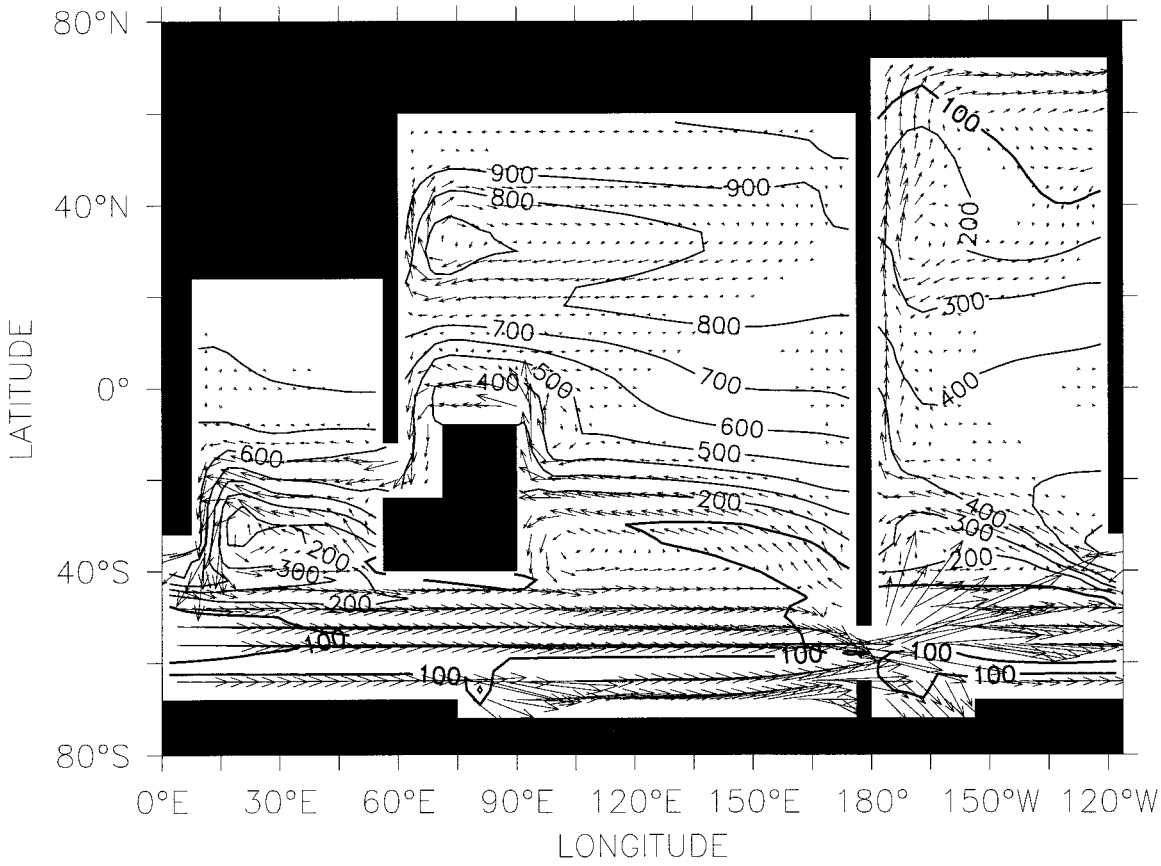

FIG. 4. Idealized ages and velocity vectors at 600 m; the contour interval is 100 yr with the 100-yr contour darkened. Maximum velocity vector is 15.67 cm s^{-1}.

estimate'' of the volume of bottom water converted into NADW, derived from water mass analyses, cited by Broecker (1991) and S95 as 4 Sv. The total outflow from the Atlantic at 30°S between 1300 and 3700 m is 15.9 Sv (8.7 Sv in the upper cell and 7.2 Sv in the lower cell), but the deep western boundary current there measures 16.6 Sv. This value is close to the S95 estimate of 18 Sv of net deep water outflow across 30°S.

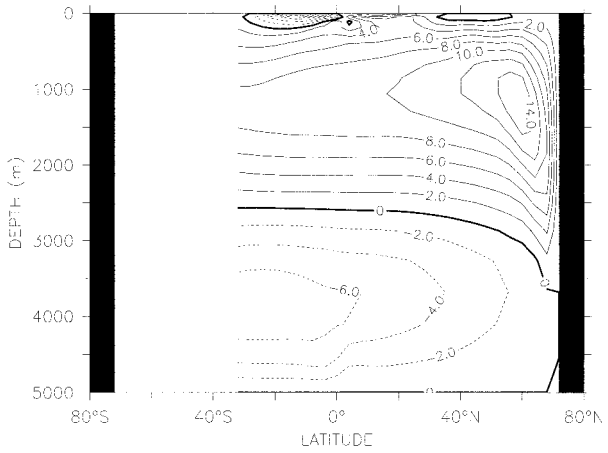

FIG. 5. Meridional overturning streamfunction for the Atlantic Ocean only; contour interval is 2 Sv. Solid (dashed) contours denote clockwise (counterclockwise) circulation. (The streamfunction is undefined south of 32°S.)

The idealized ages and velocity vectors at 2687 m are shown in Fig. 6. The water at the northern wall is under 100 years old and the strong western boundary current that carries newly formed NADW southward is apparent. Considering the idealized topography of the model, the age simulation in the Atlantic basin is quite good. The newly formed NADW matches the radiocarbon derived age ($\Delta^{14}C$) from GEOSECS [(Stuiver and Ostlund 1980; Ostlund and Stuiver 1980; Stuiver and Ostlund 1983); a map of the radiocarbon ages at 3000 m, compiled from the GEOSECS surveys, was presented in Andrée et al. (1986)]. The water is about 400 years old as it enters the ACC, slightly younger than the calculated radiocarbon age (over 500 yr) but similar to the average ages throughout the model's circumpolar region. The deep outflow from the Atlantic is replaced by an upper-level inflow from two different sources. The circulation vectors and ages in Fig. 4 show both the inflow of older water from the Indian Ocean (the Agulhas Leakage) and the inflow of younger water

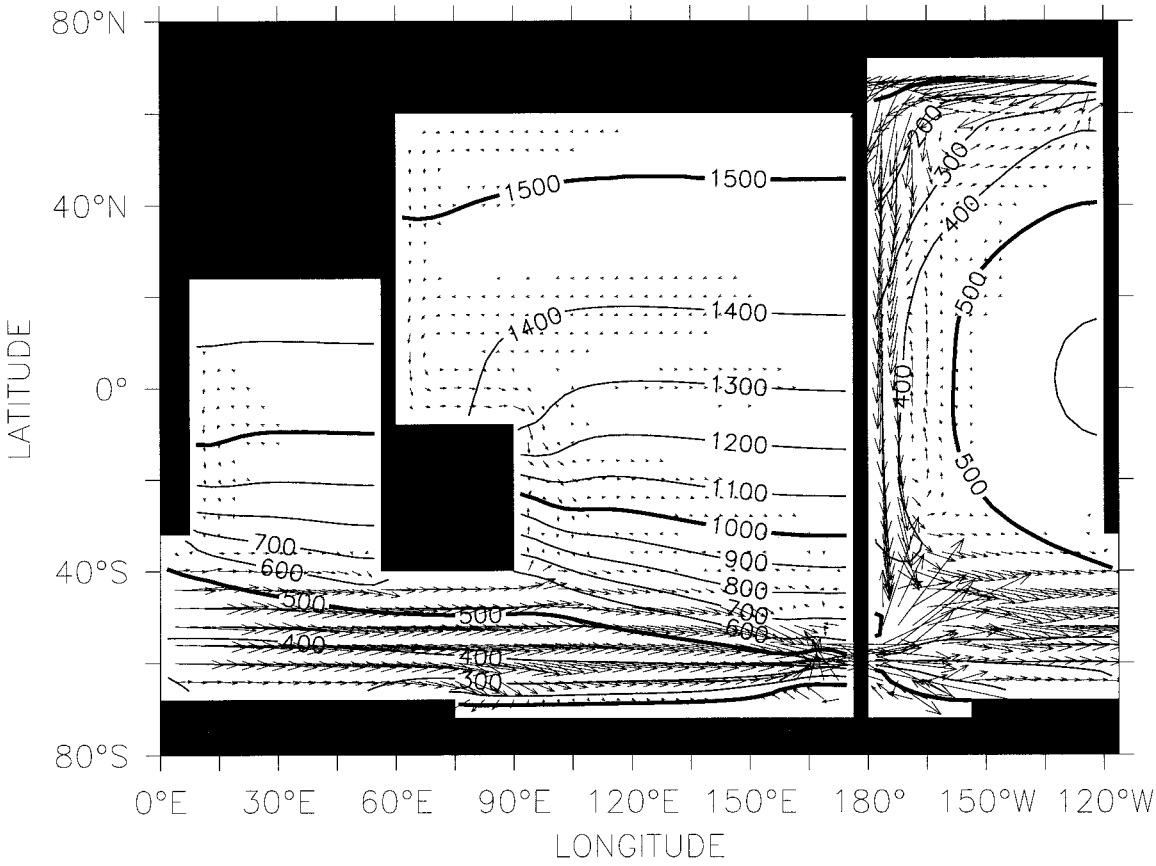

FIG. 6. Idealized ages and velocity vectors at 2687 m; the contour interval is 100 yr with the 100, 500, 1000, and 1500 yr contours darkened. Maximum velocity is 3.50 cm s^{-1}.

from the northern edge of the ACC. There is also a moderately strong northward cross-equatorial flow at this level.

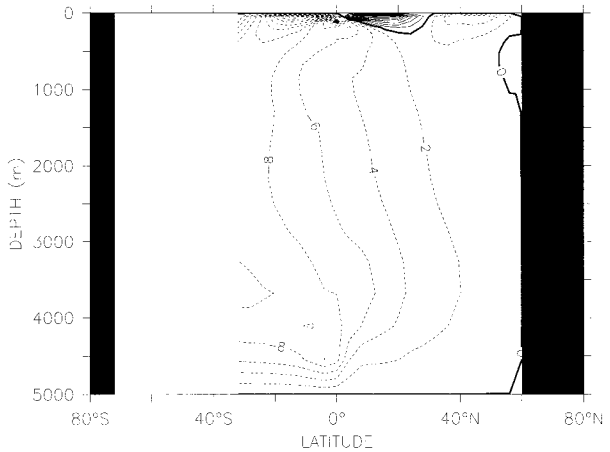

FIG. 7. Meridional overturning streamfunction for the Indian and Pacific Oceans combined; contour interval is 2 Sv. Solid (dashed) contours denote clockwise (counterclockwise) circulation. (The streamfunction is undefined south of 32°S.)

c. Indo–Pacific sector

The Pacific and Indian basins are primarily upwelling regions (Fig. 7). There is a moderate inflow of about 10 Sv along the bottom at 30°S (see also Fig. 3) and a weak net outflow at 3000 m with a total southward transport of less than 1 Sv, occurring mostly in the Indian basin (Fig. 6). The net effect of the Indian and Pacific basins north of 30°S is to convert 10 Sv of bottom water into 10 Sv of upper water. About half of the upwelling occurs north of the equator and generally the Pacific converts twice as much as the Indian basin. The model's Indo–Pacific circulation seems to be at odds with several observational studies, which conclude that there are roughly 20 $\pm$ 5 Sv of lower water converted to upper water in the Indian Ocean and very little in the Pacific Ocean (Warren 1994; S95; Macdonald and Wunsch 1996). Warren proposed that the differences in meridional overturning between the Indian and Pacific Oceans were due to a larger local heat flux over the Indian Ocean surface. This mechanism is consistent with these model results; the average heat flux at the surface in the tropical Indian is only about half that of the Pacific, despite the warmer temperatures to which the Indian surface is restored.

TABLE 2. Key sectional thermohaline component transports for the Control experiment. (Positive transport denotes eastward or northward flow; all transports in Sv.)

Location	Surface	Intermediate	Deep	Bottom
Drake Passage (E, W)	—	108.2	92.2	5.1
Atlantic basin at 30°S (N, S)	2.9	5.0	−14.4	6.5
Atlantic basin at 0° (N, S)	4.0	5.5	−15.7	6.2
Atlantic basin at 30°N (N, S)	5.5	5.3	−15.2	4.4
South of Africa (model 0°E) (E, W)	−0.9	97.5	100.6	8.3
Agulhas Leakage, N of 42°S (E, W)	−8.5	−7.8	2.6	−0.4
Indian basin at 30°S (N, S)	−17.2	−7.2	−0.9	3.1
South of Australia (model 60°E) (E, W)	11.1	113.3	102.6	0.7
Pacific basin at 30°S (N, S)	8.5	6.4	0.6	6.7
Indonesian Throughflow (E, W)	−14.6	−7.6	—	—
Pacific basin at 0° (N, S)	−4.1	−0.4	0.0	4.5
Globally averaged temperature (°C)	14.1	6.6	2.4	0.7
Globally averaged salinity (psu)	34.72	34.65	34.70	34.75
Percent of total ocean volume (%)	7.4	20.8	55.1	16.7

Several authors have reported that the bottom-water inflow into the Pacific Ocean flows out again at middepth without contacting the surface (Toggweiler and Samuels 1993; S95). Toggweiler and Samuels (1993) concluded that the magnitude of the middepth outflow was directly related to the strength of the bottom-water inflow, although their series of experiments did not include an Indonesian Throughflow. The absence of middepth outflow probably results from the lack of intermediate water production in the North Pacific; the presence of a locally formed water mass of increased density will increase the local stratification and will prevent the upwelling from below. This effect will be discussed in section 4b.

The pattern of ventilation revealed in the age profiles (Figs. 3, 4, and 6) is consistent with the observations and the model circulation. The oldest water in the model ocean is found along the northern Pacific boundary. The idealized ages are over 1500 yr between 1680 and 2760 m with a maximum of 1535 yr in the northwestern corner at 2330 m. Ages in the Indian Ocean are younger, but the maximum is still along the northern boundary (1149 yr at 1998 m in the northeastern corner). Comparing Fig. 3 with Fig. 6 shows that the ages are older at 2687 m than below at all locations in the Indian and Pacific basins, a clear sign of bottom-water upwelling. Note the bowl-shaped feature in the North Pacific at 600 m (Fig. 4), where downwelling in the subtropical gyre allows lower age surface water to diffuse down to this level. Also worth noting is the link exhibited by the circulation vectors connecting the downwelling near the southern tip of South America to the Agulhas Leakage, via the Indonesian Throughflow (Fig. 4), providing a possible pathway for the return of water into the Atlantic need to balance the deep-water export.

d. Thermohaline composite for the Control experiment

In order to examine further the model's THC and to locate those regions where water mass transformations are occurring, the movement of water in different density regimes was analyzed. The four regimes are as follows: surface water with potential density (σ_0) less than 26.5 kg m^{-3}, intermediate water with σ_0 between 26.5 and 27.5, deep water with σ_0 between 27.5 and 27.8, and bottom water with σ_0 greater than 27.8. This analysis is similar to that performed by Rintoul (1991) and Cai and Greatbatch (1995), although those studies defined deep and bottom waters solely according to model depth. The defining isopycnals for this study were chosen to delineate the model's water masses and, in that regard, this study is closer to the observational analysis of S95.

Properly speaking, this is not truly an analysis of water mass conversions, but rather a geographical census of density regimes in order to determine those locations where changes are occurring. Volume transports in the layers at various locations are given in Table 2 (similar to Table 1 in S95) and a four-diagram schematic of the volume flux for each water type in the latitude bands 80°–30°S, 30°S–0°, 0°–30°N, and 30°–80°N over each of the three ocean sectors is presented in Fig. 8.

The overall circulation in the Atlantic sector is remarkably similar to S95. Surface and intermediate water are converted into deep water in the North Atlantic where 10.8 Sv of newly downwelled water join 4.4 Sv of upwelled bottom water to form the core of the NADW mass (Figs. 8c,d). The model's upper circulation (defined as surface and intermediate water together) is about 3–4 Sv weaker than observed, which leads to the deficit between the observed 18-Sv outflow of NADW across 30°S in S95 and the model's 14.4 Sv. This is less than the mass transport of 15.9 Sv cited in section 3b because the least dense component of the southward deep western boundary current has a σ_0 less than 27.5 kg m^{-3} and is classified as intermediate water. The ~7 Sv flow of bottom water into the South Atlantic noted in section 3b is also found in the density regime analysis.

There is a large spread in the temperatures and salinities of water in the deep water regime. The average temperature and salinity for deep water in the Atlantic

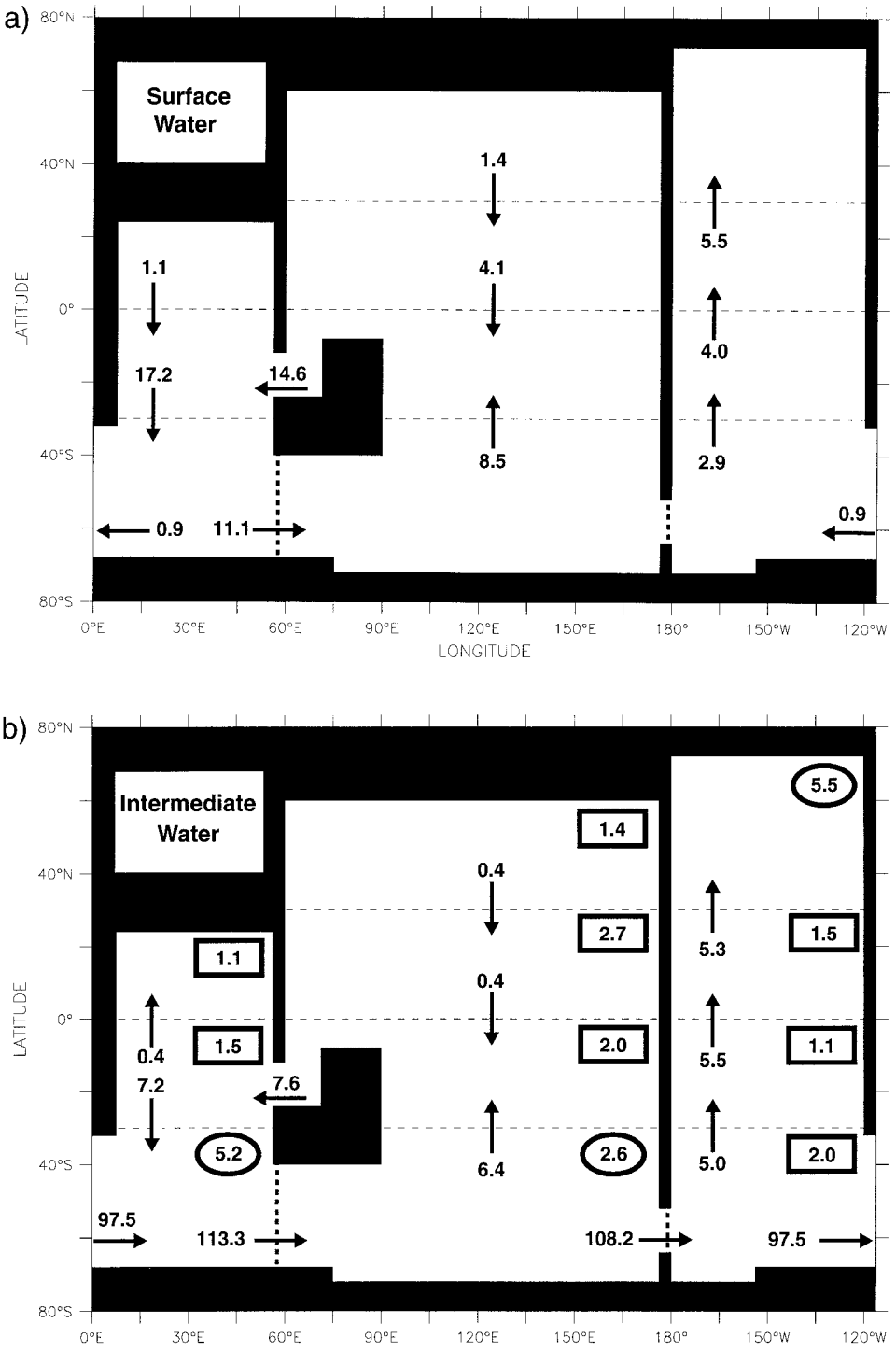

FIG. 8. This figure shows the balance for each water mass type in the control experiment for each of the three oceans within latitude bands 80°–30°S, 30°S–0°, 0°–30°N, and 30°–80°N. Arrows indicate direction of net flow and the net volume fluxes (in Sv) are noted. The figures outlined in circles (rectangles) indicate downwelling (upwelling) through the top of each box, that is, exchange with the above water mass. The four panels show (a) surface water, (b) intermediate water, (c) deep water, and (d) bottom water. [Note: The sill depth in Drake Passage at 2500 m (d) indicates that 5.1 Sv of bottom water flow through the passage above this depth.]

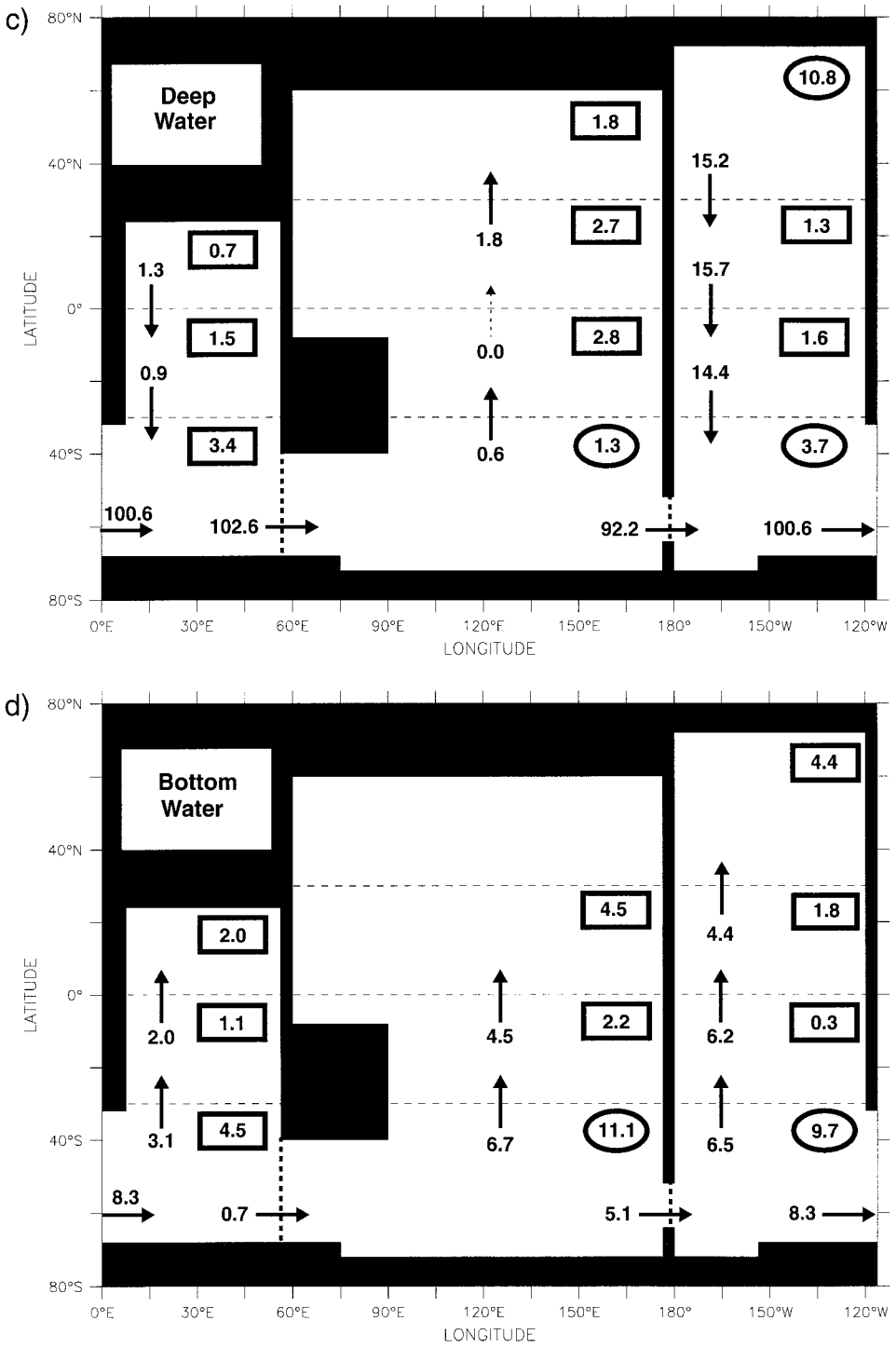

FIG. 8. (*Continued*)

basin (north of 30°S) below 1000 m are 3.3°C and 34.80 psu, whereas deep water in the Southern Ocean (south of 40°S) has values of 2.2°C and 34.71 psu. These differences agree with the observations that NADW is warmer and saltier, while the CDW shows more influence from the colder and fresher AABW. This analysis method cannot distinguish between different source regions, so it is not possible to determine the relative fraction of NADW and CDW moving across a given section. It does seem that these two water masses are somewhat separable in the South Atlantic and virtually uniform in the South Pacific, agreeing with the obser-

vation by Broecker (1991), who noted that NADW loses its unique character after only half a circuit around the Antarctic continent.

It is important to note that the only two regions in which bottom water is formed are the Atlantic and Pacific sectors of the Southern Ocean, the regions containing the two Antarctic Seas (Fig. 8d). The model continually forms 20.8 Sv of bottom water (σ_0 greater than 27.8), which upwells everywhere else as it absorbs heat diffusively from above and mixes with the overlying water masses. S95 (his Plate 9) indicates that 9 Sv of deep water are converted into bottom water in the Weddell Sea, similar to the 9.7 Sv converted in the model. Bottom-water formation in the Pacific sector of the Southern Ocean is much weaker in the model with only 11.1 Sv of net deep-water conversion, whereas the S95 analysis implies a net conversion of at least 30 Sv. The zonally integrated flow across 60°S in the lowest 1300 m is 7.9 Sv, as indicated in section 3a, and all of this flow is tagged as bottom water. There is, however, southward flow of bottom water higher in the column so that the net flow of bottom water across 60°S is only 5.8 Sv. The total bottom water transport at this latitude can be decomposed into the three geographical regimes previously discussed as follows: 15.0 Sv moving northward in the Atlantic sector, 13.3 Sv moving northward in the far-eastern Pacific, and 22.5 Sv flowing southward in the Indian and west and central Pacific.

There has been much debate about the return route of upper waters needed to compensate for the deep-water export from the Atlantic basin. The controversy rests on whether the return flow is primarily Indian Ocean water that has traveled westward around Africa through the Agulhas Leakage, known as the warm-water route, or whether the return flow is mostly Antarctic Intermediate Water from the Drake Passage, known as the cold-water route. Gordon et al. (1992), in an observational study, concluded that the return flow was primarily composed of AAIW, but a significant portion (50%–65%) was modified during a transit through the southern Indian Ocean before returning to the South Atlantic via the Agulhas Leakage in the form of baroclinic eddies, which as stated before, are not resolved by this model. The modeling study of Cai and Greatbatch (1995, hereafter CG95) also indicated the importance of AAIW but determined that at most 35% of the compensating return flow of upper water had traveled through the Agulhas Leakage. The model in CG95 was also unable to resolve the small-scale eddies and relied on the integrated flow in various density classes.

This model is compatible with the results of both Gordon et al. (1992) and CG95 with some minor discrepancies. In this study, the upper-level northward flow into the Atlantic, needed to compensate for the deep-water export, is 63% intermediate water, somewhat higher than CG95 (54%) and much higher than S95 (29%); these differences result from the choice of the defining isopycnal surface that separates surface from intermediate water. Figure 15 shows that approximately 50% of the upper return flow traveled through the Agulhas Leakage; this will be discussed further in section 4d.

A significant difference between the model and the observational analysis is the generally weak flow of bottom waters into the Pacific basin and the subsequent lack of deep water outflow, as discussed previously. Figure 8c indicates a net flux of 0.6 Sv of deep water moving northward across 30°S; this conceals a recirculation of approximately 6 Sv but is not at all similar to the 20 Sv of deep water outflow reported in S95. No water with σ_0 greater than 27.8 kg m^{-3} crosses 10°N in the model Pacific, consistent with the Levitus (1982) climatology, which also shows no water greater than this density in the bottom 1000 m of the central or northern Pacific. Wijffels et al. (1996) reported that 8 Sv of lower CDW with a potential temperature below 1.2°C crosses 10°N from the south, but no water in the model's deep Pacific is this cold. It should also be noted that the Pacific and Indian basins north of 30°S, as well as the tropical Atlantic (between 30°S and 30°N), are entirely upwelling regions.

Veronis (1975) showed that coarse-resolution OGCMs suffer from anomalous upwelling on the coastal side of western boundary currents. As Böning et al. (1995) point out, this anomalous upwelling is largely responsible for the deficit in both deep-water outflow and northward heat transport. This model does indeed exhibit a weak Veronis effect, but its existence does not greatly affect the results presented in this section. Except in the North Atlantic, the surface western boundary currents in the wind-driven gyres are confined to the upper 1000 m of the water column and so are contained entirely within the intermediate and surface water regimes above the 27.5 kg m^{-3} isopycnal surface. The Veronis effect may alter the balance between intermediate water and surface water, but this distinction is not crucial to the results presented here. In the Atlantic basin, the northward flowing Gulf Stream does extend below this isopycnal, but the upwelling across it, south of 30°N, is less than 0.8 Sv. North of 30°N, the Veronis effect reduces the net creation of deep water; at 60°N, 14.7 Sv of intermediate water flow northward and 16.4 Sv of deep water flow southward, implying that 1.2 Sv of deep water are lost due to this effect between 60° and 30°N.

Drijfhout et al. (1996) employed a particle tracking method to determine where water downwelled in the North Atlantic was last below 1500 m. Their results indicate that 27% of the water had upwelled in the Atlantic Ocean, 14% in the Indian Ocean, 43% in the Pacific Ocean, and 16% in the Southern Ocean. Their model circulation, however, did not include an Agulhas Leakage, and their Indonesian Throughflow was only about 2 Sv, which will effect the results of the back-calculated particle trajectories. Although it is not possible to differentiate between NADW and CDW in this

experiment, the net gain of 15.8 Sv of deep water (conversion from the intermediate regime) in the model is balanced by a positive buoyancy forcing induced loss of 18% in the Atlantic, 14% in the Indian, 46% in the Pacific, and 22% in the Southern Ocean (Fig. 8c).

Unlike the analysis of the overturning circulations alone, the density regime analysis reveals that most of the positive buoyancy-forced water mass conversion (from denser to lighter, typically equated with upwelling) occurs in the equatorial band between 30°S and 30°N. This region accounts for over 57% of the upwelling of bottom water, 66% of the upwelling of deep water, and 74% of the upwelling of intermediate water. The strong vertical transports in the Antarctic sector are mostly associated with recirculations and not water mass conversions. It is possible that the limited zonal extent of these simulations (240°) leads to an underestimation of the wind-driven upwelling of deep water in the ACC. Further studies are needed, but it seems likely that convection and the surface forcing in this region would keep the balance between intermediate and deep water roughly constant.

4. No-NADW experiment

In order to evaluate the effects of NADW on the global ocean circulation, an experiment without this water mass was conducted and the results of the two experiments are compared. Sedimentary evidence from the last glacial period seems to indicate that NADW production was severely reduced, if not eliminated entirely, at the last glacial maximum (Boyle and Keigwin 1987). Several studies have described and compared global circulations both with and without NADW (Manabe and Stouffer 1988; Stocker et al. 1992; Power and Kleeman 1993; CG95). All employed global models but generally limited the scope of their analyses. This study's focus is on the global THC, but the changes reported in those previous works will be compared to this one.

Rather than try to duplicate the glacial ocean by forcing the model with the poorly known glacial climatology, this study limits its scope to studying the effects of reduced NADW formation. This is accomplished by imposing a negative 1‰ salinity anomaly into the restoring salinity values of the Control experiment over the Atlantic basin north of 40°N. The salinity forcing outside of this region remains unchanged, as do temperature and wind stress values everywhere. The model is then run until a new steady state is reached (about 6000 yr). It should be noted that the final state of the ocean in this No-NADW experiment did not depend on the initial conditions; the anomalous salinity forcing was applied to both an isothermal ocean at rest and to the final steady state of the Control experiment—the results were identical.

Some of the effects of NADW production on the global circulation are visible by comparing Fig. 2 and Fig. 9. The most obvious change is that there is no longer any deep-water formation in the northern hemisphere (Fig. 9a). Apart from the surface Ekman cells, the overturning circulation north of the equator is much weaker than in the southern hemisphere. Figure 2d shows that the elimination of NADW causes the model's globally averaged temperature in the upper 2300 m to warm, by over 0.5°C at 500 m, while the bottom 2700 m cool slightly (by 0.25°C at 3500 m). The surface salinity anomaly north of 60°N in the North Atlantic severely reduces the average (maximum) convective depth there from 1400 (4100) m to 400 (1100) m (compare Figs. 2b and 9b). There is also an increase in the convection in the Southern Ocean when NADW is eliminated; the 500-m contour expands between 40° and 60°S, and the 1000-m contour shifts farther away from the Antarctic coast. Figure 2e shows that the removal of NADW causes the global salinity to decrease at all levels, including a change of over 0.1‰ between 700 and 3800 ms. The causes and effects of these changes will be discussed in the next section.

The ACC transport has increased from 205.5 to 235.1 Sv and the Indonesian Throughflow and the barotropic Agulhas Leakage are both about 2 Sv weaker (Figs. 9c, d). The structure of the Agulhas Leakage is modified by the presence of NADW; without this water mass, the westward transport in the upper 1000 m is reduced from 15.1 to 9.0 Sv. The westward flow below this depth, however, increases from 1.2 to 3.7 Sv and extends down to 3000 m, compared to the 1550-m level when NADW production is active. The decrease in transport through the Indonesian passage and the decreased upper-level transport around the tip of Africa are both consistent with the ''warm-water route'' of the conveyor-type circulation proposed by Broecker and Gordon. Figure 9d shows that the horizontal streamfunctions for both experiments are identical north of the equator. Since there is no bottom topography in the model's northern hemisphere, the JEBAR term is identically zero and the barotropic streamfunction (or more accurately, the vertically integrated vorticity equation) is solely a function of the wind forcing (Holland 1973; Mertz and Wright 1992), which is the same in both model runs.

a. Antarctic sector

The net Antarctic downwelling in the southernmost grid box has been reduced by one-third from over 27 Sv (Fig. 2a) to just over 18 Sv (Fig. 9a). Nearly all of this reduction in the net downwelling is actually due to an increased upwelling in the southwestern and central Ross Sea. The downwelling regions in the Weddell Sea and the southeastern Ross Sea are virtually unchanged. The change in the Antarctic overturning circulation is due to a complex series of interactions involving the ACC. The absence of the comparatively saline NADW outflow reduces the salinity below 1000 m at the northern edge of the ACC throughout the southern subpolar ocean. Reduced salinity lowers the density of the water

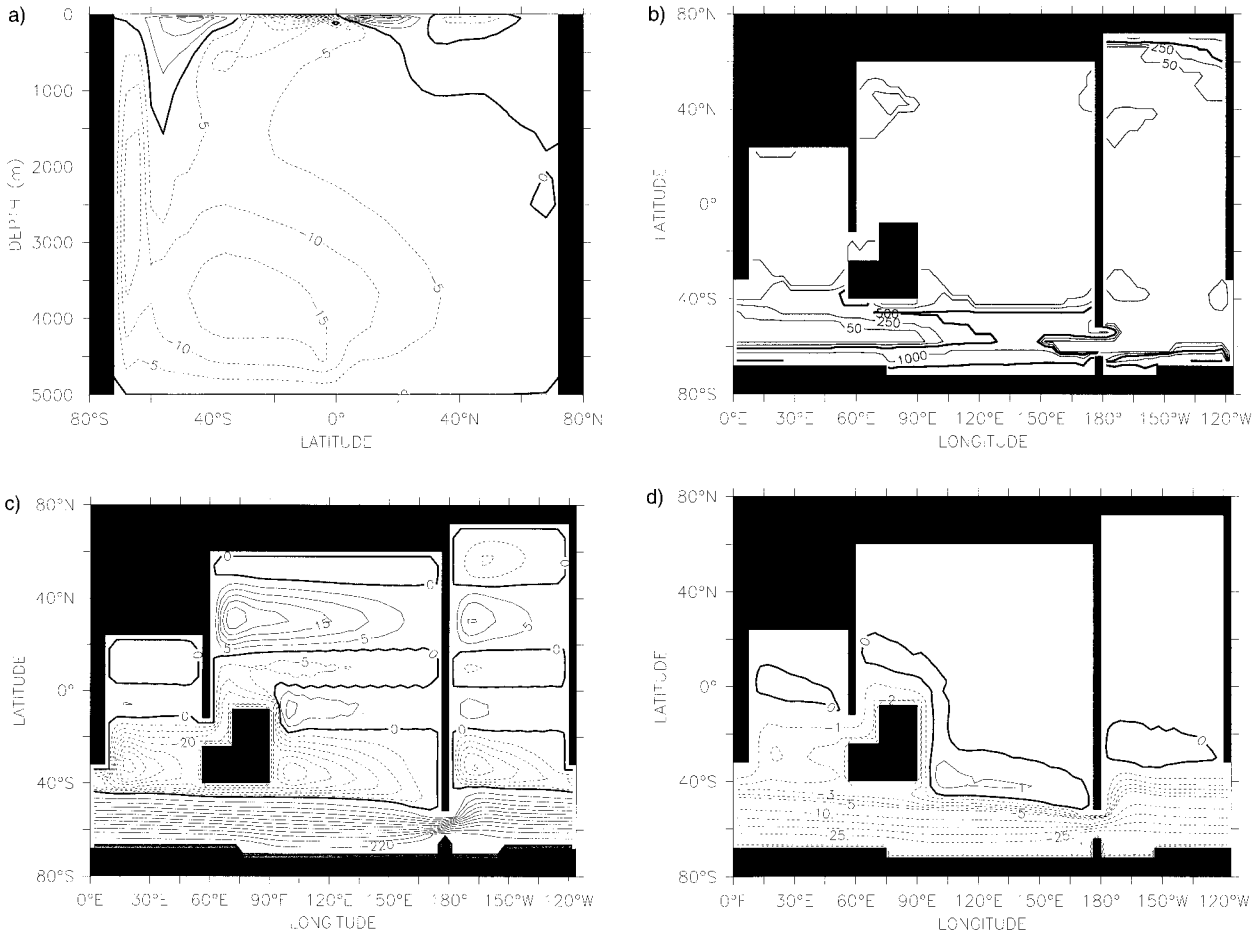

FIG. 9. No-NADW experiment: (a) Meridional overturning streamfunction; contour interval is 5 Sv. (b) Depth of convection from the surface; contours at 50, 250, 500, 1000, 2500, and 5000 m, with the 500- and 2500-m contours darkened. (c) Barotropic streamfunction; contour interval is 5 Sv, except in the ACC where it is 20 Sv. (d) Change in the barotropic streamfunction due to the production of NADW (Control experiment − No-NADW experiment); contour interval is 5 Sv in the ACC and 1 Sv elsewhere. Note that in (a), (c), and (d) solid (dashed) contours denote clockwise (counterclockwise) circulation.

at and above the depth of the Drake Passage sill on the northern edge, while the density at the southern edge of the ACC is closely bound to the surface restoring profile and has not changed. These effects combine to increase the density gradient across the ACC, which increases the baroclinity of the flow and acts through the JEBAR term in the vorticity equation (Mertz and Wright 1992) to increase the strength of the barotropic transport through Drake Passage by 14% in the No-NADW experiment. This change is similar to the one seen in CG95; their ACC increases from 202.9 to 233.3 Sv when NADW formation is cut off.

Nearly all of the change in the Antarctic overturning seen by comparing Figs. 2a and 9a occurs in the Indo–Pacific sector. The enhanced ACC in the No-NADW experiment leads to greater convergence at the northwestern tip of the Antarctic Peninsula. Increased horizontal convergence in a weakly stratified region leads to vertical motion in the model, which in this case is increased downwelling. As in the control experiment, most of the vertical motion between 68° and 60°S in the No-NADW experiment is still upward, but the sinking at the tip of the peninsula increases by over 8 Sv, while the rest of the region continues to upwell at the same rate in both experiments. Some of the increased downward flow feeds an increased export of AABW into the southeastern Pacific, and the rest of this extra downwelling eventually upwells in the southwestern Ross Sea. So despite the appearance of a weakened South Antarctic overturning in the No-NADW experiment, the vertical transports, both upward and downward, are intensified. The net zonal overturnings south of 60°S in the No-NADW experiment for the Indo–Pacific and Atlantic sectors, which are hidden by the zonal integral, are 66 and 36 Sv (again, measured at 2500 ms), respectively, compared to 55 and 27 Sv in the Control experiment.

The average heat flux (out of the ocean) south of 60°S increases very slightly (~0.6 W m^{-2}) when NADW is removed, but the equivalent salt flux (the net evapo-

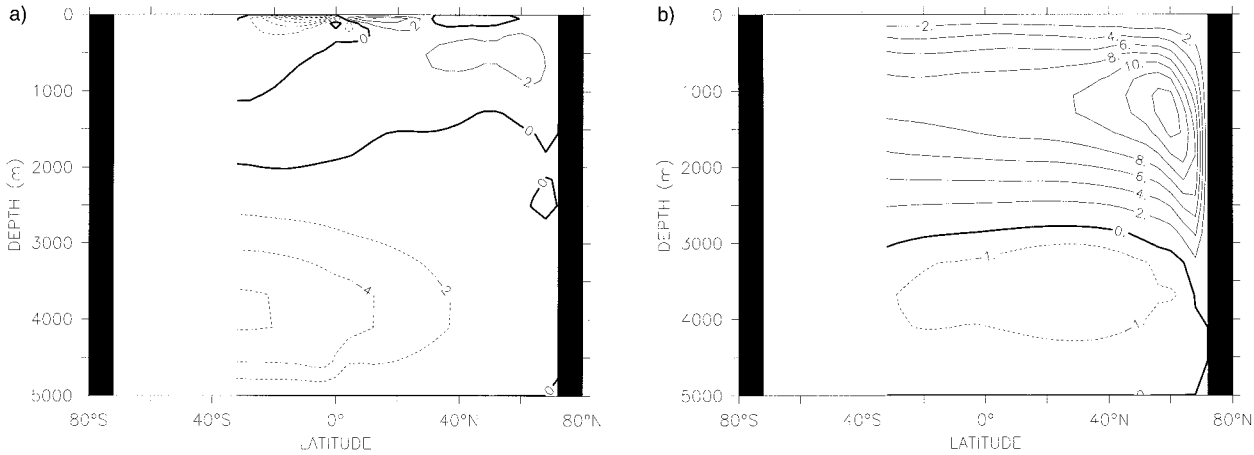

FIG. 10. (a) No-NADW experiment meridional overturning streamfunction for the Atlantic Ocean only. (b) Change in meridional overturning due to NADW production (control experiment − No-NADW experiment). Contour interval in both figures is 2 Sv, with the −1 contour included in (b). Solid (dashed) contours denote clockwise (counterclockwise) circulation. (The streamfunction is undefined south of 32°S.)

ration minus precipitation, which can be thought of as ice export) into the ocean increases substantially from 0.06 to 0.32 m yr^{-1} to balance the lack of southward salt transport by NADW. These differences are also explained by the increase in convection in the No-NADW experiment; the restoring boundary condition has to work harder when more deep water is ''exposed'' to the surface.

Despite the reduction in the net downwelling at the southern wall in the absence of NADW production, the increase in total downwelling leads to an increase in the northward flow across 60°S in the bottom 1300 m from 7.9 Sv in the Control experiment to 10.4 Sv in the No-NADW experiment. Comparing the three regimes discussed in section 3a, the increased outflow across 60°S is confined to the region between 165°E and the American continent. The northward meridional flow at the bottom in the Atlantic sector decreases by a small amount (~0.8 Sv), and the southward meridional flow into the southwestern and central Ross Sea increases slightly.

Circumpolar Deep Water is the end product of strong mixing in the ACC. In the Control experiment, it is composed of the three main subsurface water masses, AABW, NADW, and AAIW. When NADW is missing, the new CDW is generally much fresher and a bit colder; this causes a decrease in its density at all levels and reduces the stratification in the ACC above 1500 m. The increased convection along with the increased convergence at the northern edge of the ACC causes the production (and volume) of AAIW to increase substantially. This inverse correlation between the production of AAIW and NADW seems consistent with the study of Michel et al. (1995), although their main conclusion, that subantarctic convection formed the global deep-water mass during the glacial period, is not seen in the model.

In summary, NADW production has four main effects on the Antarctic region: 1) the ACC transport is weaker when NADW is present, 2) the downwelling and upwelling in the high-latitude Southern Ocean are both decreased in magnitude when NADW is present, 3) the net outflow of bottom water across 60°S is weakened when NADW is present although the outflow in the Atlantic sector increases slightly, and 4) the formation of AAIW is reduced when NADW is present.

b. Atlantic sector

The changes to the Atlantic overturning are obvious and fairly easy to explain (compare Figs. 5 and 10a). The northern overturning is restricted to the upper 1500 m and is reduced from 15.8 Sv to just over 3 Sv. In the No-NADW experiment, less than 1 Sv of surface water from the North Atlantic flows southward across 30°S between 1500 and 2000 m. The bottom cell transport is reduced by 1 Sv, but bottom water now upwells to 2000 m before exiting the basin to the south. The dense NADW mass, owing primarily to its salt content, suppresses the upwelling of bottom water by 1000 m between the two model runs.

Figure 10b shows that an extra 8.6 Sv of water from south of 30°S are drawn into the basin, flow northward across the equator, and return southward at depth after passing through the North Atlantic sinking region. This affects the stratification in the Atlantic basin, as expected. The influx of upper water needed to supply the downwelling in the north comes from the Southern Ocean as AAIW and Agulhas Leakage water. This water is generally colder than the tropical water present at upper levels in the No-NADW experiment, leading to a cooling of upper ocean. At depth, NADW replaces AABW, leaving the deep ocean warmer in the Control experiment. These changes increase the stratification in the upper ocean above 1500 m and weaken it below there. The northward heat transport in the Atlantic in-

creases from 0.16 PW in the No-NADW experiment to 0.52 PW in the Control experiment. This increase of 0.36 PW in the heat transport is seen at all latitudes between 30°S and 40°N, implying that thermal energy from the Southern Ocean is released to the atmosphere over the North Atlantic, equivalent to an additional 26 W m^{-2} of heating north of 40°N. Notice that NADW formation also causes an increase in the flow of bottom water through the basin, as was indicated in the previous section.

Figure 10a gives a clue as to why the model's Pacific Ocean does not produce a middepth outflow of bottom water as is seen in the observations. Even with the negative salinity anomaly imposed on the North Atlantic, the surface density is still large enough for the water to sink to intermediate depths, whereas the model's Pacific surface water is too light. Yasuda (1997) concluded that North Pacific Intermediate Water (NPIW) is largely composed of cold, low-salinity water from the Sea of Okhotsk mixed with some warmer, saltier water from the western subarctic gyre. The lack of Okhotsk Sea mode water (Yasuda 1997), and thus NPIW, in the model decreases the stratification in this region and allows bottom water to upwell without constraint to the surface, whereas even the artificial North Atlantic Intermediate Water in the No-NADW experiment is enough to cap the upwelling of bottom water, thus causing it to flow southward out of the basin.

An interesting finding is that the salinity balance in the upper North Atlantic is between the northward advection of salt by the Gulf Stream and the convective mixing with deep water, consistent with the results of Manabe and Stouffer (1988). In both the control and the No-NADW experiments, the restoring boundary condition in the model removes salt from (rains on) the North Atlantic surface. In the No-NADW run, despite the reduced restoring salinity, the amount of salt removed is significantly less than in the Control run due to the large reduction in advective transport by the Gulf Stream. The model ''rains'' more (equivalent to removing more salt) there when NADW is formed, implying that the high surface salinities in the model North Atlantic are due to the existence of the thermohaline overturning and not to the restoring salinity boundary condition. Manabe and Stouffer (1988) also determined that the difference between evaporation and the sum of precipitation and runoff was virtually identical in their coupled model, in both the NADW and No-NADW experiments. It is notable, however, that their salinity flux adjustment, which removes the equivalent of 5 m per year of surface water in the North Atlantic near Iceland, is not enough to induce convection and deep-water formation there, apparently due to the lack of poleward salinity advection in their Gulf Stream.

It is informative to present the age differences caused by NADW formation. Figure 11 shows the differences due to the presence of NADW (the Control experiment minus the No-NADW experiment). At 2687 m (the same level as Fig. 6, immediately below the Drake Passage sill), the ventilating effects of NADW are most dramatic in the North Atlantic. In the No-NADW case, water at this depth is ventilated slowly from the south and achieves an age of almost 1000 yr. The rejuvenating effect of NADW proceeds southward along the western boundary and then into the ACC. CDW at this level is between 100 and 200 years younger when NADW is included. The circulation carries the younger water into the Indian basin where it gradually spreads northward and eastward. The strong bullet of refreshed water along the southeastern coast of Australia is due to a reversal of the current from southward in the No-NADW experiment to northward in the Control case, which replaces older deep Pacific water with younger CDW at that location. This reversal is an effect of the large change in the density of CDW. In the Control experiment, CDW is much denser than the deep Pacific water at this level, but the two are nearly identical in the No-NADW experiment.

c. Indo–Pacific sector

The Indo–Pacific overturning is similar in both experiments. Comparing Figs. 7 and 12a shows that the inflow along the bottom is weaker when NADW formation is active (Fig. 12b) and less of the bottom flow eventually crosses the equator. It is important to note that the North Pacific (north of about 20°N) is slightly older when NADW production is active, and this is true along the bottom as well, where ages are 0–30 years older north of the equator (Figs. 11 and 13b). The ventilation time of the water in this location is determined primarily by the strength of the bottom-water influx. The bottom water is of southern origin (AABW and/or CDW) in both experiments, so NADW production can only influence the bottom ages through a dynamical process. The small reduction in the flow of bottom water across the equator in the Pacific and Indian basins causes their deepest waters to age slightly. The changes in ventilation times in the Pacific and Indian sectors, due to the formation of NADW, are between −350 and 150 yr everywhere.

There is an increased inflow between 1500 and 3500 m due to NADW formation (Fig. 12b), equally divided between the two basins, which increases the total upper-level upwelling by about 2 Sv. Not coincidentally, the Indonesian Throughflow is also 2 Sv stronger in the Control experiment than in the No-NADW experiment (Fig. 9d). The link between the strength of the Indonesian Throughflow and the production of NADW has been explored by several studies (Gordon et al. 1992; Hirst and Godfrey 1993; Macdonald and Wunsch 1996) with inconclusive results.

An interesting result is that both the Pacific and Indian Oceans are warmer below 2500 m and colder above when NADW production is active (Fig. 13a), with a decrease of over 0.5°C between 300 and 1500 m. The

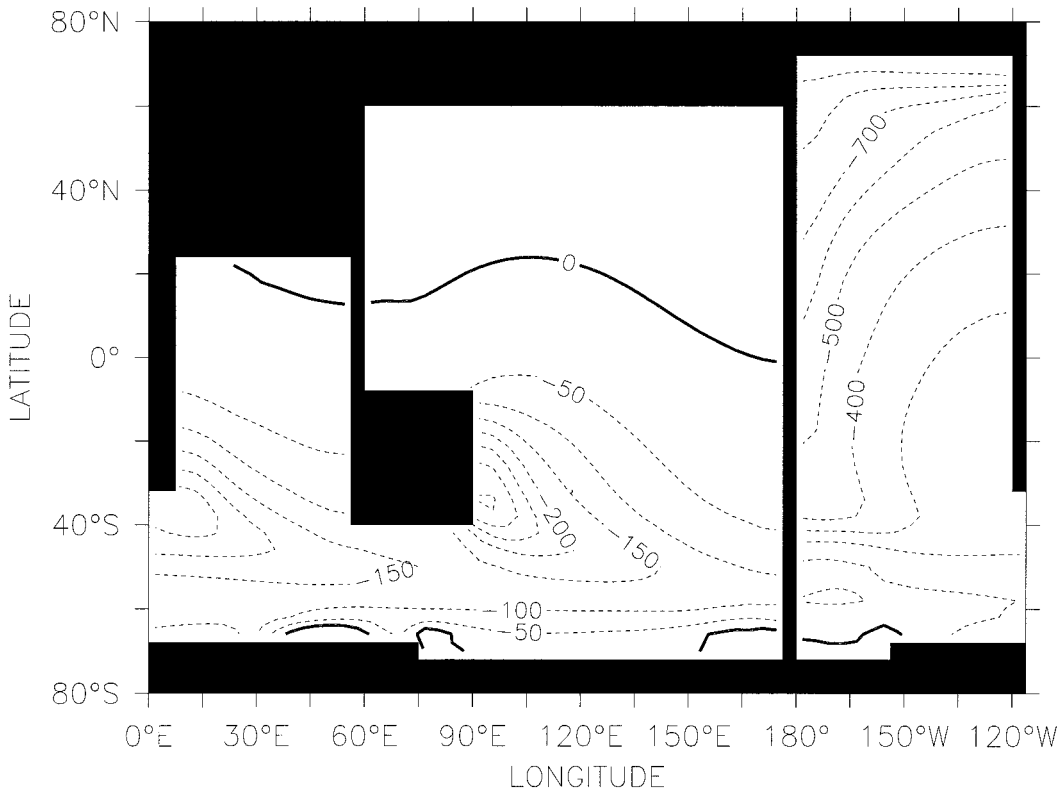

FIG. 11. The change in age at 2687 m due to the production of NADW (Control experiment − No-NADW experiment). The contour interval is 100 yr in the Atlantic sector and 50 yr in the Indian and Pacific sectors.

warming at depth is due to the incorporation of relatively warm NADW into the CDW, which is advected into the northern basins. The changes to the ACC noted in section 4a, however, result in less formation of intermediate water, which leaves the upper circumpolar region slightly colder. This cooling is generally not advected northward across 40°S because the main flows at this level are southward (Fig. 12b). The heat balance in the tropical and extratropical Indian and Pacific basins is between the downward diffusion of solar radiation absorbed at the surface and the upwelling of cold water from below the thermocline; upwelling increases in the model when NADW is present, so the upper-level temperature goes down. This subsurface cooling is ex-

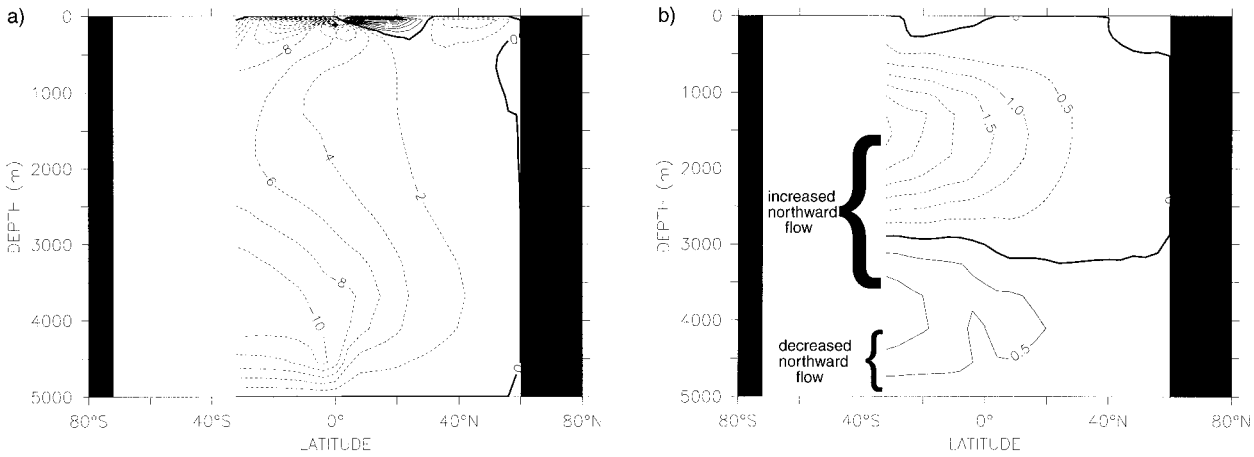

FIG. 12. (a) No-NADW experiment meridional overturning streamfunction for the Indian and Pacific Oceans combined. (b) Change in meridional overturning due to NADW production (Control experiment − No-NADW experiment). Contour interval in (a) is 2 Sv and in (b) is 0.5 Sv. Solid (dashed) contours denote clockwise (counterclockwise) circulation. (The streamfunction is undefined south of 32°S.)

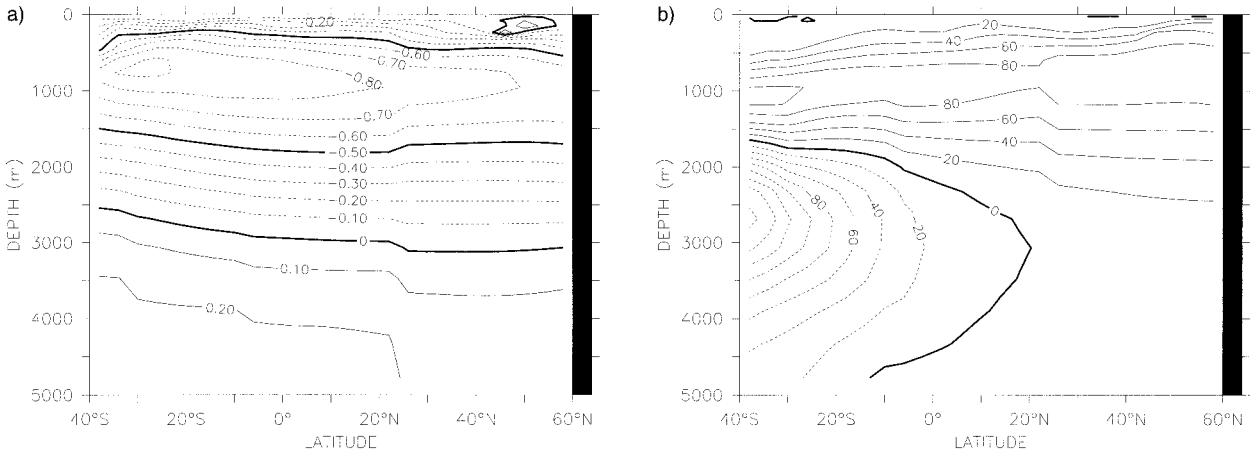

FIG. 13. Zonally averaged changes in the Indian and Pacific Oceans due to NADW production (Control experiment − No-NADW experiment). (a) Change in temperature; contour interval is 0.1°C with the −0.5°C contour darkened. (b) Change in idealized age; contour interval is 20 yr.

pressed at the surface, but only weakly due to the surface forcing. The thermal boundary condition restores the model's tropical SST to the same profile in both experiments, but the downward heat flux through the surface is slightly larger in the Control experiment. If a different thermal boundary condition were implemented, such as the Schopf zero-heat capacity atmosphere (Schopf 1983), the tropical SSTs in the No-NADW experiment would be noticeably warmer than in the Control experiment.

This conflicts with the evidence indicating that tropical SSTs in the last glacial period were about 5°C colder (Rind and Peteet 1985; Thompson et al. 1995; Stute et al. 1995) despite the absence of NADW formation. This coarse-resolution model cannot begin to resolve the tropical surface heat budget, but the model results presented here imply that the SST differences observed during the glacial period were the result of atmospheric effects, and not the ocean circulation. Manabe and Stouffer (1988) found that NADW formation caused warming (cooling) over the entire northern (southern) hemisphere, both in the model SST and in the model surface air temperature. It seems clear that the coupled model allows SST anomalies to be redistributed via the atmosphere throughout the model domain, which is not possible here.

It is notable that the thermal structure and the age structure of the upper Pacific and Indian Oceans are determined by the same factors. While NADW production causes the deep Indian and Pacific Oceans to become younger below about 2000 m due to the rejuvenated CDW (with its NADW component) that flows in at depth (Fig. 13b), the increased upwelling in the upper ocean (above 2500 m) causes the ages there to increase. This change is in agreement with the δ^{13}C evidence reported in Duplessy and Labeyrie (1994), which indicated that Pacific intermediate waters between 1000 and 2600 m were more ventilated (younger) during the last glaciation. The largest cooling of the upper equatorial Indian and Pacific Oceans occurs over the same depths as the increase in ages.

d. Thermohaline composite for the No-NADW experiment

The analysis performed on the Control experiment in section 3d was also carried out for the No-NADW experiment. Although the globally averaged salinity drops from 34.72 psu in the Control run to 34.60 psu in the No-NADW run, and the average σ_0 decreases from 27.46 to 27.35 kg m^{-3}, the same four density ranges were used for comparison. Table 3 gives volume transports for each water mass across the various sections, and Fig. 14 is the corresponding schematic and should be compared to Fig. 8.

An obvious change is the sharp reduction in bottom water formation from 20.8 to 12.3 Sv and the total absence of water with σ_0 greater than 27.8 kg m^{-3} north of the equator (Fig. 14d). Although there is no net production in the Atlantic sector of the Southern Ocean, convection in the Weddell Sea (south of 68°S) does convert just under 10 Sv of deep to bottom water but all of it upwells south of 30°S. All the water located on the bottom is still southern in origin (Fig. 14c), but most is now less than 27.8 kg m^{-3}. Due to the nonlinearity in the equation of state for seawater, the changes in salinity have a much greater effect on the density at low temperatures than do changes in the temperature. Without the conduit created by convection in the North Atlantic, the salinity throughout the World Ocean decreases and the low temperature of water along the bottom away from the coast of Antarctica is no longer sufficient for those waters to be classified as ''bottom water'' based on the potential density.

The biggest change is in the volume of intermediate water (compare Tables 2 and 3); the net conversion of

TABLE 3. Key sectional thermohaline component transports for the No-NADW experiment. (Positive transport denotes eastward or northward flow. All transports in Sv.)

Location	Surface	Intermediate	Deep	Bottom
Drake Passage (E, W)	—	168.2	66.9	—
Atlantic basin at 30°S (N, S)	−2.0	1.6	−2.7	3.1
Atlantic basin at 0° (N, S)	0.1	−0.5	0.4	—
Atlantic basin at 30°N (N, S)	1.8	−2.1	0.3	—
South of Africa (model 0°E) (E, W)	4.3	147.6	86.3	−3.1
Agulhas Leakage, N of 42°S (E, W)	−4.0	−8.2	0.3	—
Indian basin at 30°S (N, S)	−14.9	−6.2	0.9	—
South of Australia (model 60°E) (E, W)	13.2	152.3	102.1	−12.3
Pacific basin at 30°S (N, S)	9.0	5.2	6.0	—
Indonesian Throughflow (E, W)	−12.6	−7.6	—	—
Pacific basin at 0° (N, S)	−3.7	−0.2	3.9	—
Globally averaged temperature (°C)	14.4	5.7	1.6	0.1
Globally averaged salinity (psu)	34.72	34.51	34.58	34.71
Percent of total ocean volume (%)	8.4	32.5	56.5	2.6

surface to intermediate water south of 30°S is greater by about 2.1 Sv when NADW is absent. This is largely due to the increase in the ACC transport and the resulting horizontal convergence at the western coasts of Australia and South America. The depth of convection in the Southern Ocean between 60° and 40°S is about 20% deeper, and the stratification there and throughout the rest of the World Ocean is notably weaker above 1400 ms without the influence of NADW. The 27.5 kg m^{-3} isopycnal surface is deeper everywhere when NADW is absent, ranging from about 500 m deeper in the Pacific and Indian Oceans to 900 m or more in the Atlantic. Most of the change in intermediate water is due to the replacement of diffusively warmed, high-salinity upper NADW by low-salinity AAIW. The global salinity drops by about 0.1‰, and the largest decrease occurs around the depth of the 27.5 kg m^{-3} isopycnal surface in the Control run, causing upper deep water to be reclassified as lower intermediate water. There is still intermediate water formation in the North Atlantic (Fig. 14b) but its effects south of the equator are small or nonexistent.

Most of the changes in net transport between Figs. 14c,d and 8c,d in the Indian and Pacific Oceans are due to an increase in the broad southward flows (the deep outflow discussed earlier), while the total northward flows in the deep western boundary currents remain fairly constant. The increased deep outflow is also revealed in the reduced upper-level upwelling.

The change in the strength of the Agulhas Leakage between the two runs is used to estimate the percentage of upper water compensating for NADW outflow, which has traveled through the Indian sector, as was done by CG95. Their Agulhas Leakage is 3.7 Sv weaker when NADW is absent and nearly all of the reduction occurs in the intermediate water. The westward flow of intermediate water in the present study actually increases by 0.4 Sv when NADW is removed but the surface flow is reduced by 4.5 Sv for a net reduction of 4.1 Sv. Some of these differences are due to the criteria used to differentiate between intermediate and surface water; CG95 levels have a lower depth of 1250 m for intermediate water and when their criteria are applied to the current study, much of the westward flowing intermediate water is reclassified as deep water. The ratio of the change in the Agulhas Leakage to the upper (surface and intermediate) return flow into the Atlantic is 36% in CG95 and 52% here.

5. Summary and conclusions

A simplified cartoon depicting the major aspects of the model's thermohaline circulation is presented in Fig. 15. NADW formation causes several distinct changes in the World Ocean's structure and circulation patterns, but the production of Antarctic Bottom Water in the model is not dependent on NADW production. Vertical motion in the high-latitude Southern Ocean is divided into three main regions: downwelling across the Atlantic sector and in a narrow band in the Pacific immediately west of the Antarctic Peninsula and broad upwelling in the southern Indian and southwestern Pacific sectors. The flow of bottom water across 60°S is divided into the same three regimes; newly downwelled water (AABW) flows northward across the Atlantic and in the far-eastern Pacific, while older (and warmer) circumpolar water flows southward to feed the broad upwelling in the southern Indo–Pacific sector. This feature is robust in both experiments and is a strong indication that NADW formation alone does not drive the model's global thermohaline overturning. The strength of AABW formation and the northward flow of bottom water across 60°S are affected, however, by the transport in the ACC; NADW formation influences the Southern Ocean through this intermediary.

In the No-NADW experiment, all three northern basins behave quite similarly and the thermohaline circulation is fairly simple. Nearly all subsurface water-mass production occurs in the Southern Ocean. The densest water is formed near Antarctica, sinks to the bottom, and flows northward into each basin where it warms diffusively and upwells slowly. In the Atlantic

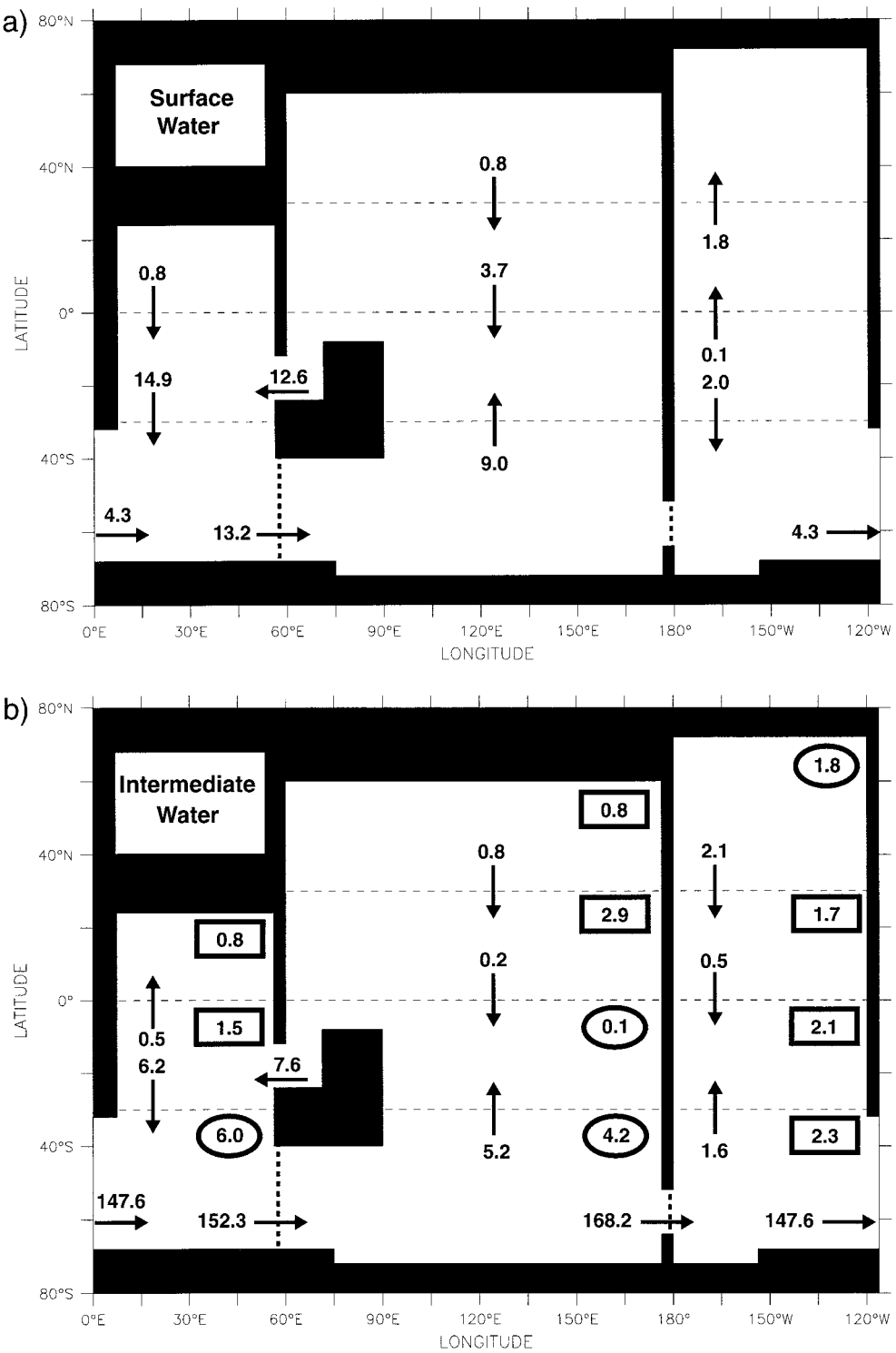

FIG. 14. This figure shows the balance for each water mass type in the No-NADW experiment for each of the three oceans within latitude bands 80°–30°S, 30°S–0°, 0°–30°N, and 30°–80°N. Arrows indicate direction of net flow and the net volume fluxes (in Sv) are noted. The figures outlined in circles (rectangles) indicate downwelling (upwelling) through the top of each box, that is, exchange with the above water mass. The four figures show (a) surface water, (b) intermediate water, (c) deep water, and (d) bottom water.

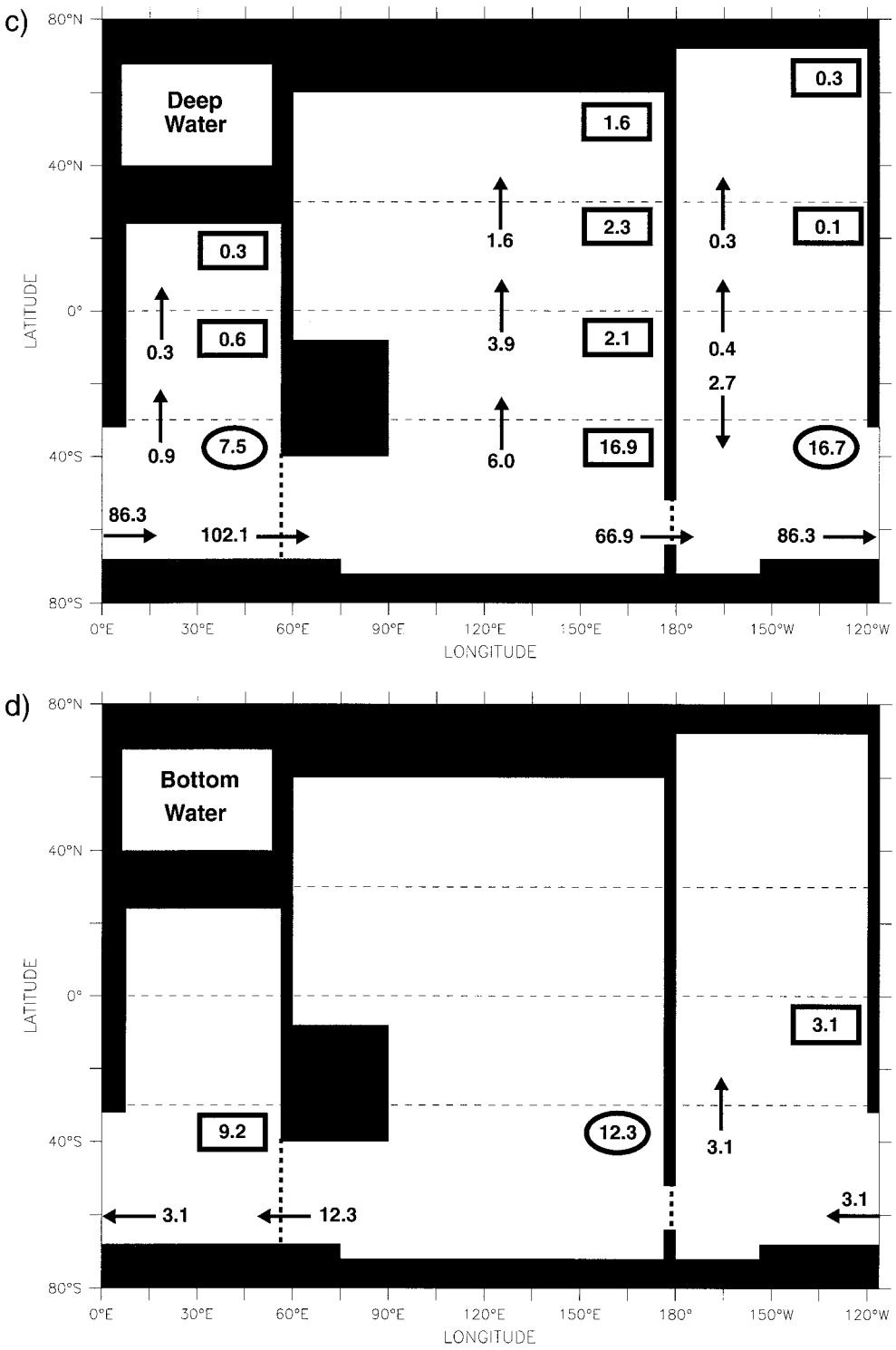

FIG. 14. (*Continued*)

Ocean, all of the bottom water exits southward, rejoining the ACC as upper deep water. In the Indian and Pacific Oceans, some bottom water is recirculated and rejoins the ACC, but most continues to warm, becoming intermediate and then surface water. Low-salinity intermediate water of southern origin also fills the upper levels of the three northern basins; all three have an equatorial salinity minimum located between 1000- and

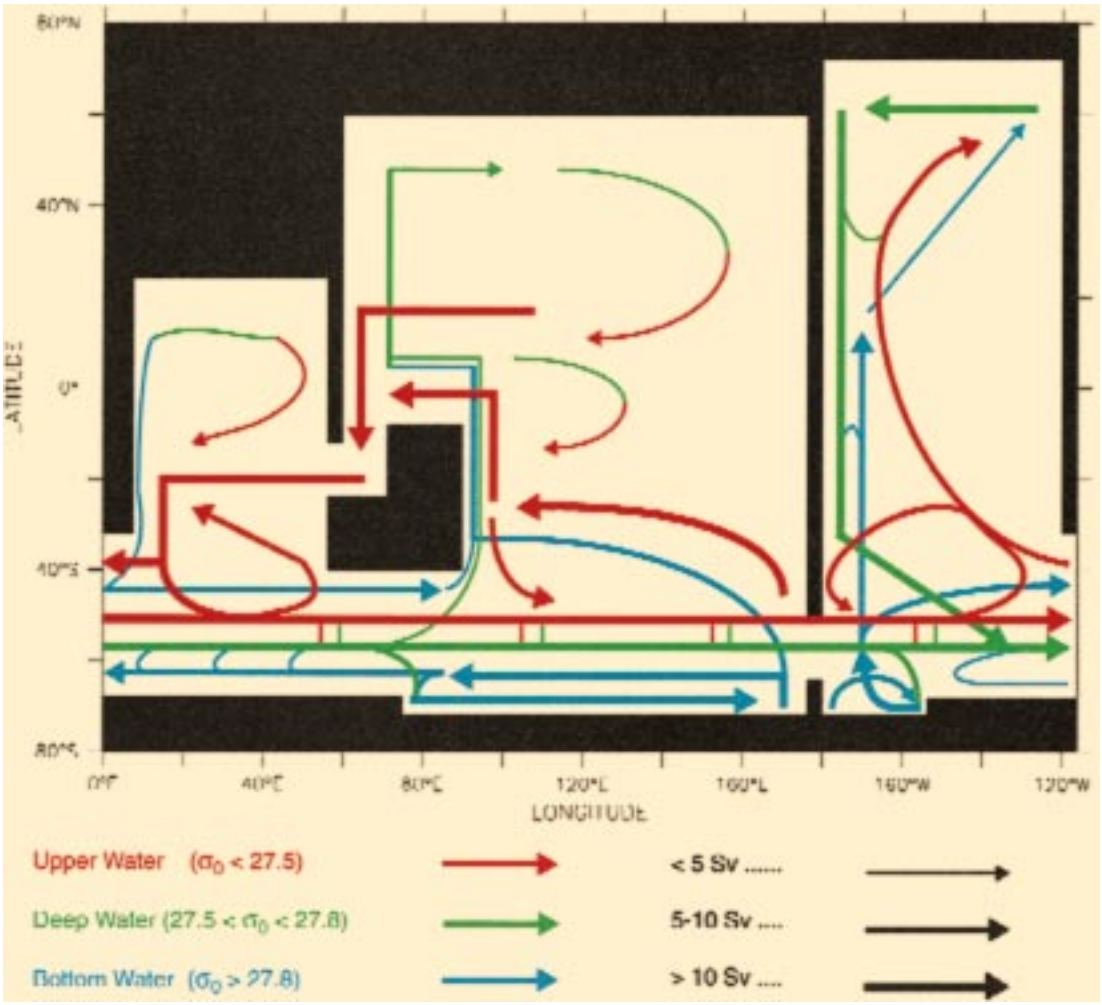

FIG. 15. Cartoon of the model's conveyor belt circulation for the control experiment. The colors describe flows in terms of density ranges and location in the water column: red arrows indicate the combined surface and intermediate flows, green arrows indicate deep flow, and blue arrows indicate bottom flow. Note that the flow depicted by the blue arrows adjacent to Antarctica indicate an eastward surface flow of roughly the same density as the flow depicted by the westward blue arrows next to them.

2000-m depth. The Pacific and Atlantic both have low-salinity surface water at their northern extreme, but only the northern Atlantic is cold enough for the low-salinity water at the surface to sink into the water column. This weak North Atlantic Intermediate Water formation moderates the deep Atlantic ages slightly and increases the local stratification, preventing the upwelling of bottom water to the surface. The age structure of the three northern basins in the No-NADW experiment all have their oldest water between 2000 and 3000 m along the northern wall.

In the Control experiment, the higher restoring salinity increases the convective mixing in the high-latitude North Atlantic, which overturns nearly 16 Sv down to 3500 m, causing a restructuring of the Atlantic branch of the THC. The upper-level flow (above 1000 m) in the Gulf Stream at 30°N in the western Atlantic increases by about 13 Sv, all of which eventually sink and return southward in the deep western boundary current. Despite the prescribed increase in surface salinity, the net precipitation north of 50°N at equilibrium in the Control experiment is less than in the No-NADW experiment; the extra surface salt is delivered by the enhanced Gulf Stream, not by the restoring boundary condition. The northward heat transport in the Atlantic basin increases by over 0.35 PW, all of which is released to the atmosphere north of 40°N, providing an additional 26 W m^{-2} of heating over the northern Atlantic. A net of 14 Sv of NADW flows southward across 30°S out of the basin. This outflow is replaced by 6 Sv of southern bottom water and 8 Sv of upper water. The upper-level compensation in this study is evenly divided between the warm- and cold-water routes as is indicated in Fig. 15.

The high-latitude convection in the North Atlantic provides a pathway for tropical heat and salt into the

deep ocean. The deep outflow from the northern sinking region advects a large quantity of salt southward that leads to an increased density at the northern edge of the ACC and a decreased density gradient across the ACC. This reduces the baroclinic component of the flow through the JEBAR term in the vorticity equation and thereby reduces the total transport through the Drake Passage. The net effect of NADW on the high-latitude Southern Ocean overturning is to decrease both the downwelling and the upwelling in the Indo–Pacific sector; downwelling decreases due to reduced horizontal convergence at the northwestern tip of the Antarctic Peninsula, and upwelling decreases due to reduced convergence along the bottom in the central Ross Sea. The northward flow of bottom water across 60°S is decreased when NADW present, and this decrease is largely confined to the far-eastern Pacific region (less Antarctic downwelling and less northward flow).

In both of the model experiments presented here, the Indian and Pacific basins are upwelling regions. There is, however, no a priori reason why this should be so. If the atmospheric circulation were to change in a way that altered the net hydrological cycle, it could be possible for the northern Pacific to form intermediate (as it already does in reality in the Sea of Okhotsk) or deep water and thus alter its branch of the thermohaline circulation. These experiments have shown that changing the Atlantic circulation has only a small effect on the meridional circulations in the Pacific and Indian Oceans. Rather than a single, unified ''conveyor belt,'' the global THC seems more modular; each high-latitude basin functions quasi-independently, responding to its own heat and salinity balance. New subsurface water masses spread out from their formation regions and compete for space in the water column according to their relative density, mediated through intense mixing in the circumpolar region. Further study is needed to establish the nature of the relationship and the effects of subsurface water mass creation in the different regions of the global ocean.

NADW formation reduces the ventilation time of the deep Atlantic by over 900 yr at the northern boundary. The age reduction due to this water mass decreases as it flows southward; water at 30°S and 2500-m depth is between 250 and 500 yr younger in the control experiment than in the No-NADW experiment. Outside of the Atlantic basin, the effect of NADW on the ventilation time of the deep ocean decreases dramatically after NADW enters the ACC. The low age signal of NADW is blended into the Circumpolar Deep Water and is then advected into the Indian and Pacific basins. Dynamically, the reduced northward flow of water from the circumpolar region below 4000 m, which accompanies NADW production, causes those northern areas ventilated by bottom water to age, especially in the North Pacific. The decreased deep outflow (roughly between 1500 and 3500 m) from the Indian and Pacific Oceans in the Control experiment leads to increased upper-level upwelling, which alters the upper-level age balance. The heat balance and the age balance in the upper ocean are governed by the same factors: the downward diffusion of surface tracers becomes less effective due to the enhanced upwelling, leading to both increased ages and decreased temperatures. Most of the model's deep ocean, outside of the Atlantic basin, experiences less than a 10% change in its age due to NADW production.

The deep Pacific and Indian basins are ventilated by a combination of AABW, CDW, and NADW flowing in from the south. The model's CDW is made up of the denser components of a recirculated mixture of all the subsurface water masses present in the Southern Ocean. When CDW includes the NADW component, its density increases due to its higher salinity, but its movement throughout the model ocean is only slightly affected. Denser CDW does increase the stratification in the upper Southern Ocean and reduces the formation of southern subpolar intermediate water (AAIW). Globally, NADW production causes the entire ocean to become denser with the largest increase occurring at about 1200-m depth. This effect causes an increase in the stratification above this level and a decrease in the stratification below. The increase in upper-level stratification reduces the downward diffusion of surface properties and leads to generally colder and less ventilated upper waters.

The age structure of the model ocean derived from the passive age tracer is dependent on the number and strength of subsurface water mass formation regions and can serve as a useful tool for comparing different ocean modeling efforts. The ventilation timescales derived from this tracer are highly dependent on the vertical diffusivity employed; further refinements to the models as well as additional observational study will narrow our uncertainties about the overturning timescale of the World Ocean.

The two experiments highlight a critical distinction that is generally lacking in the discussion of the global circulation. Most of the upwelling in the model (the upward vertical movement of water parcels) occurs in the Southern Ocean, while most of the positive buoyancy forcing associated with the THC (converting the denser subsurface water masses back into lighter ones) occur in the Tropics. The latter is primarily associated with the downward diffusion of heat and this process is strongest near the equator.

Acknowledgments. The author would like to thank Drs. E. S. Sarachik, D. A. McDermott, and J. Ribbe, as well as the two anonymous reviewers, for their comments on this paper. I also wish to thank the Pacific Marine Environmental Laboratory for providing me with Ferret, a diagnostics and graphics program, which has been used intensively in this study. All the figures in this work, except for the cartoon, were produced with Ferret. This work was supported by a grant from the

NOAA/Office of Global Programs to the Stanley P. Hayes Center of the University of Washington.

REFERENCES

Andrée, M., H. Oeschger, W. Broecker, N. Beavan, M. Klas, A. Mix, G. Bonani, H. J. Hoffman, M. Suter, W. Woelfli, and T.-H. Peng, 1986: Limits on the ventilation rate for the deep ocean over the last 12,000 years. *Climate Dyn.,* **1,** 53–62.

Böning, C. W., W. R. Holland, F. O. Bryan, G. Danabasoglu, and J. C. McWilliams, 1995: An overlooked problem in model simulations of the thermohaline circulation and heat transport in the Atlantic Ocean. *J. Climate,* **8,** 515–523.

Boyle, E. A., and L. Keigwin, 1987: North Atlantic thermohaline circulation during the past 20,000 years linked to high-latitude surface temperature. *Nature,* **330,** 35–40.

Broecker, W. S., 1987: The biggest chill. *Natural History Magazine,* **97,** 74–82.

——, 1991: The great ocean conveyor. *Oceanography,* **4,** 79–89.

——, 1995: Chaotic climate. *Sci. Amer.,* **273,** 62–68.

——, T.-H. Peng, S. Trumbore, G. Bonani, and W. Wolfli, 1990: The distribution of radiocarbon in the glacial ocean. *Global Biogeochem. Cyc.,* **4,** 103–117.

——, S. Blanton, W. M. Smethie Jr., and G. Ostlund, 1991: Radiocarbon decay and oxygen utilization in the deep Atlantic Ocean. *Global Biogeochem. Cyc.,* **5,** 87–117.

Bryan, K., and L. J. Lewis, 1979: A water mass model of the world ocean. *J. Geophys. Res.,* **84,** 2503–2517.

Cai, W., and R. J. Greatbatch, 1995: Compensation for the NADW outflow in a global ocean general circulation model. *J. Phys. Oceanogr.,* **25,** 226–241.

Carmack, E. C., and T. D. Foster, 1975: On the flow of water out of the Weddell Sea. *Deep-Sea Res.,* **22,** 711–724.

Cox, M. D., 1989: An idealized model of the world ocean. Part I: The global-scale water masses. *J. Phys. Oceanogr.,* **19,** 1730–1752.

Drijfhout, S. S., E. Maier-Reimer, and U. Mikolajewicz, 1996: Tracing the conveyor belt in the Hamburg large-scale geostrophic ocean general circulation model. *J. Geophys. Res.,* **101,** 22 563–22 575.

Duffy, P. B., and K. Caldeira, 1997: Sensitivity of simulated salinity in a three-dimensional ocean model to upper ocean transport of salt from sea-ice formation. *Geophys. Res. Lett.,* **24,** 1323–1326.

Duplessy, J.-C., and L. Labeyrie, 1994: Surface and deep water circulation changes during the last climatic cycle. *Long-Term Climatic Variations,* J. C. Duplessy and M. T. Spyridakis, Eds., NATO ASI Series, Springer-Verlag, 277–298.

——, N. J. Shackleton, R. G. Fairbanks, L. Labeyrie, D. Oppo, and N. Kallel, 1988: Deep water source variations during the last climatic cycle and their impact on the global deep water circulation. *Paleoceanography,* **3,** 343–360.

——, M. Arnold, E. Bard, L. Labeyrie, J. Duprat, and J. Moyes, 1992: Glacial-to interglacial changes in ocean circulation, *Radiocarbon After Four Decades,* R. E. Taylor, A. Long, and R. S. Kra, Eds., NATO ASI Ser., Springer-Verlag, 62–74.

England, M. H., 1993: Representing the global-scale water masses in ocean general circulation models. *J. Phys. Oceanogr.,* **23,** 1523–1552.

——, 1995: The age of water and ventilation timescales in a global ocean model. *J. Phys. Oceanogr.,* **25,** 2756–2777.

Fichefet, T., S. Hovine, and J.-C. Duplessy, 1994: A model study of the Atlantic thermohaline circulation during the last glacial maximum. *Nature,* **372,** 252–255.

Fieux, M., R. Molcard, and A. G. Iiahude, 1996: Geostrophic transport of the Pacific–Indian Oceans throughflow. *J. Geophys. Res.,* **101,** 12 421–12 432.

Foster, T. D., 1995: Abyssal water mass formation off the eastern Wilkes Land coast of Antarctica. *Deep-Sea Res.,* **42,** 501–522.

——, and E. C. Carmack, 1976: Frontal zone mixing and Antarctic Bottom Water formation in the southern Weddell Sea. *Deep-Sea Res.,* **23,** 301–317.

Gent, P. R., and J. C. McWilliams, 1990: Isopycnal mixing in ocean circulation models. *J. Phys. Oceanogr.,* **20,** 150–155.

Gordon, A. L., 1986: Interocean exchange of thermocline water. *J. Geophys. Res.,* **91,** 5037–5046.

——, 1991: The role of the thermohaline circulation in global climate change. Annual Report 1990–1991, Lamont-Doherty Earth Observatory, Columbia University, Palisades, New York, 44–51 [Available from LDEO, Box 1000, 61 Route 9W, Palisades, NY 10964-1000.]

——, R. F. Weiss, W. M. Smethie Jr., and M. J. Warner, 1992: Thermocline and intermediate water communication between the South Atlantic and Indian Oceans. *J. Geophys. Res.,* **97,** 7223–7240.

Haidvogel, D. B., and F. O. Bryan, 1992: Ocean general circulation modeling. *Climate System Modeling,* K. E. Trenberth, Ed., Cambridge University Press, 371–412.

Haney, R. L., 1971: Surface thermal boundary condition for ocean circulation models. *J. Phys. Oceanogr.,* **1,** 241–248.

Hellerman, S., and M. Rosenstein, 1983: Normal monthly wind stress over the world ocean with error estimates. *J. Phys. Oceanogr.,* **13,** 1093–1104.

Hirst, A. C., and J. S. Godfrey, 1993: The role of Indonesian throughflow in a global ocean GCM. *J. Phys. Oceanogr.,* **23,** 1057–1086.

Holland, W. R., 1973: Baroclinic and topographic influences on the transport in western boundary currents. *Geophys. Fluid Dyn.,* **4,** 187–210.

Hughes, T. M. C., and A. Weaver, 1994: Multiple equilibria of an asymmetric two-basin ocean model. *J. Phys. Oceanogr.,* **24,** 619–637.

Levitus, S., 1982: *Climatological Atlas of the World Ocean,* NOAA Prof. Paper No. 13, U. S. Govt. Printing Office, Washington, D.C., 173 pp.

Macdonald, A. M., and C. Wunsch, 1996: An estimate of global ocean circulation and heat fluxes. *Nature,* **382,** 436–439.

Manabe, S., and R. J. Stouffer, 1988: Two stable equilibria of a coupled ocean–atmosphere model. *J. Climate,* **1,** 841–866.

Mantyla, A. W., and J. L. Reid, 1983: Abyssal characteristics of the World Ocean waters. *Deep-Sea Res.,* **30,** 805–833.

Marotzke, J., and J. Willebrand, 1991: Multiple equilibria of the global thermohaline circulation. *J. Phys. Oceanogr.,* **21,** 1372–1385.

Mertz, G. and D. G. Wright, 1992: Interpretations of the JEBAR term. *J. Phys. Oceanogr.,* **22,** 301–305.

Meyers, G., 1996: Variation of Indonesian throughflow and the El Nino–Southern Oscillation. *J. Geophys. Res.,* **101,** 12 255–12 263.

Michel, E., L. D. Labeyrie, J.-C. Duplessy, N. Gorfti, M. Labracherie, and J.-L. Turon, 1995: Could deep subantarctic convection feed the world deep basins during the last glacial maximum. *Paleoceanography,* **10,** 927–942.

Ostlund, H. G., and M. Stuiver, 1980: GEOSECS Pacific radiocarbon. *Radiocarbon,* **22,** 25–53.

Pacanowski, R. C., K. Dixon, and A. Rosati, 1991: The GFDL modular ocean model users guide, version 1.0, GFDL Ocean Group Tech. Rep. 2, 376 pp. [Available from GFDL, Box 308, Route 1, Princeton, NJ 08542.]

Peacock, S. L., and W. S. Broecker, 1998: The Southern Ocean deep water production dilemma. *J. Geophys. Res.,* in press.

Power, S. B., and R. Kleeman, 1993: Multiple equilibria in a global ocean general circulation model. *J. Phys. Oceanogr.,* **23,** 1670–1681.

Rind, D., and D. Peteet, 1985: Terrestrial conditions at the last glacial maximum and CLIMAP sea-surface temperature estimates: Are they consistent? *Quat. Res.,* **24,** 1–22.

Rintoul, S. R., 1991: South Atlantic interbasin exchange. *J. Geophys. Res.,* **96,** 2675–2692.

Robitaille, D. Y., and A. J. Weaver, 1995: Validation of sub-grid scale

mixing schemes using CFC's in a global ocean model. *Geophys. Res. Lett.,* **22,** 2917–2920.
Schmitz, W. J., 1995: On the interbasin-scale thermohaline circulation. *Rev. Geophys.,* **33,** 151–173.
Schopf, P. S., 1983: On equatorial waves and El Nino. II: Effects of air–sea thermal coupling. *J. Phys. Oceanogr.,* **13,** 1878–1893.
Semtner, A. J., Jr., and R. M. Chervin, 1988: A simulation of the global ocean circulation with resolved eddies. *J. Geophys. Res.,* **93,** 15 502–15 522.
Shriver, J. F., and H. E. Hurlburt, 1997: The contribution of the global thermohaline circulation to the Pacific to Indian Ocean throughflow via Indonesia. *J. Geophys. Res.,* **102,** 5491–5511.
Speer, K. G., and W. Zenk, 1993: The flow of Antarctic Bottom Water into the Brazil Basin. *J. Phys. Oceanogr.,* **23,** 2667–2682.
Stocker, T. F., D. G. Wright, and W. S. Broecker, 1992: The influence of high-latitude surface forcing on the global thermohaline circulation. *Paleoceanography,* **7,** 529–541.
Stuiver, M., and H. G. Ostlund, 1980: GEOSECS Atlantic radiocarbon. *Radiocarbon,* **22,** 1–24.
——, and ——, 1983: GEOSECS Indian Ocean and Mediterranean radiocarbon. *Radiocarbon,* **25,** 1–29.
Stute, M., M. Forster, H. Frischkorn, A. Serejo, J. F. Clark, P. Schlosser, W. S. Broecker, and G. Bonani, 1995: Cooling of tropical Brazil (5°C) during the last glacial maximum. *Science,* **269,** 379–383.
Thompson, L. G., E. Mosley-Thompson, M. E. Davis, P.-N. Lin, K. A. Henderson, J. Cole-Dai, J. F. Bolzan, and K.-B Liu, 1995: Late glacial stage and Holocene tropical ice core records from Huascaran, Peru. *Science,* **269,** 46–50.
Toggweiler, J. R., and B. Samuels, 1993: New radiocarbon constraints on the upwelling of abyssal water to the ocean's surface. *The Global Carbon Cycle,* M. Heimann, Ed., NATO ASI Series, Springer-Verlag, 333–366.
——, and ——, 1995: Effect of sea ice on the salinity of Antarctic bottom waters. *J. Phys. Oceanogr.,* **25,** 1980–1997.
Veronis, G., 1975: The role of models in tracer studies. *Proc. Numerical Models of Ocean Circulation,* Durham, NH, Ocean Science Committee of the Ocean Affairs Board, 133–145.
Warren, B. A., 1994: Driving the meridional overturning in the Indian Ocean. *Deep-Sea Res.,* **41,** 1349–1360.
Weaver, A. J., and M. Eby, 1997: On the numerical implementation of advection schemes for use in conjunction with various mixing parameterizations in the GFDL ocean model. *J. Phys. Oceanogr.,* **27,** 369–377.
Whitworth, T., III, W. D. Nowlin Jr., and S. J. Worley, 1982: The net transport of the Antarctic circumpolar current through Drake Passage. *J. Phys. Oceanogr.,* **12,** 960–971.
Wijffels, S. E., J. M. Toole, H. L. Bryden, R. A. Fine, W. J. Jenkins, and J. L. Bullister, 1996: The water masses and circulation at 10°N in the Pacific. *Deep-Sea Res.,* **43,** 501–544.
Yasuda, I., 1997: The origin of North Pacific Intermediate Water. *J. Geophys. Res.,* **102,** 893–909.